mathematics

MDPI

Article

Analysis of U-V2X Communications with Non-Clustered and Clustered Jamming in the Presence of Fluctuating UAV Beam Width

Mohammad Arif * and Wooseong Kim *

Department of Computer Engineering, Gachon University, Seongnam-si 13120, Republic of Korea
* Correspondence: mohammadarif911@gachon.ac.kr (M.A.); wooseong@gachon.ac.kr (W.K.)

Abstract: Jammers emit strong intentional jamming signals aiming to limit or block legitimate communications. The distribution of jammers, whether in non-clustered or clustered form, significantly influences the performance of vehicle-to-everything (V2X) networks. In addition, the fluctuations in the three-dimensional (3D) antenna beam width of unmanned aerial vehicles (UAVs) can exert a substantial impact on the network's overall performance. This paper introduces a model for UAV-V2X (U-V2X) communications in mm-Wave bands, considering non-clustered and clustered jammers, as well as the varying 3D antenna beam width. The roads are modeled using a Poisson line process, vehicular nodes (VNs) are modeled using a 1D Poisson point process (PPP), and UAVs are modeled using a 3D PPP. The jammers are distributed in two ways: non-clustered and clustered distributions. Moreover, the fluctuations in the 3D antenna beam width follow a normal distribution. To this end, a typical node's performance in U-V2X communications is evaluated for various network configurations, including the number of UAVs, VNs, roads, jammers, and jammer's transmission power. The analytical expressions for the outage probability (OP) of VN to VN connection (i.e., V2V), VN to UAV connection (i.e., V2U2V), and an overall connection (i.e., U-V2X), under non-clustered and clustered jamming, along with the fluctuating antenna beam width, are derived. The results revealed that the performance of the U-V2X communications utilizing mm-Waves is significantly degraded with the non-clustered jamming in comparison with the clustered jamming. The fluctuations in the 3D beam width of the UAV antennas further compromise the network's performance. Thus, accurate modeling of these fluctuations is crucial, particularly in the presence of non-clustered jammers. Furthermore, the system designers should focus on implementing additional anti-jamming countermeasures specifically targeting non-clustered jammers in U-V2X communications.

Keywords: jamming; V2X communications; unmanned aerial vehicles; MCP; PPP

MSC: 60D05

Citation: Arif, M.; Kim, W. Analysis of U-V2X Communications with Non-Clustered and Clustered Jamming in the Presence of Fluctuating UAV Beam Width. *Mathematics* **2023**, *11*, 3434. https://doi.org/10.3390/math11153434

Academic Editor: Jonathan Blackledge

Received: 17 July 2023
Revised: 5 August 2023
Accepted: 6 August 2023
Published: 7 August 2023

1. Introduction

Jammers intentionally produce signals to interfere with legitimate communications. The disruption created by the jammers, which can result in signal deterioration, communication failures, or reduced network performance, is referred to as jamming interference. Jamming interference compromises the performance of various applications in vehicle-to-everything (V2X) communications. For instance, jamming signals can disrupt the signals transmitted by ambulances or fire brigades requesting neighboring vehicles for enhanced safety and emergency response. Similarly, jamming signals can disrupt the performance of advanced driver assistance systems, such as warning for collision avoidance, detection for blind spots, assistance for lane change, and safety at junctions.

The third-generation partnership project (3GPP) supports various modes of reliable communication by unmanned aerial vehicle (UAV) V2X (U-V2X) networks such as vehicle-to-vehicle, vehicle-to-UAV, vehicle-to-infrastructure, and vehicle-to-pedestrian, as shown in

Figure 1 [1–4]. U-V2X communications improve network outage and SE performance by deploying UAVs over critical roads or highways for various applications such as autonomous driving in vehicular platooning [5,6] and for entertainment or disseminating emergency messages in internet of vehicles [7]. This addresses system reliability and connectivity, specifically in the aftermath of natural disasters where conventional wireless infrastructure is disrupted, as well as during events such as concerts or sports matches, where the network is overloaded with extensive data traffic.

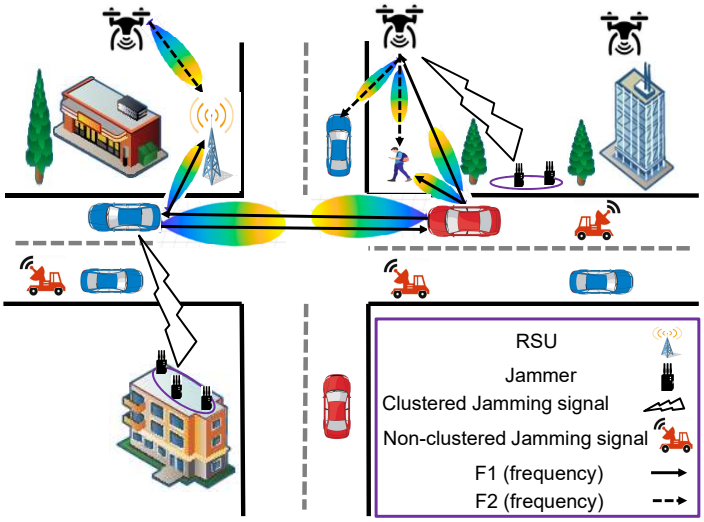

Figure 1. Non-clustered and clustered jammers in a U-V2X network.

1.1. Related Works

Jamming in U-V2X communications can compromise vehicular-node (VN)-to-VN mode communication (i.e., exchange of information in VNs, e.g., vehicles, road-side units (RSUs), and pedestrians) or VN-to-UAV mode communication (i.e., exchange of information between VNs and UAVs). Jamming in U-V2X communications can be broadly categorized as non-clustered jamming (NCJ) and clustered jamming (CJ). NCJ is a form of jamming in which the jammers are dispersed throughout the given area without displaying an organized clustering structure. In this situation, the jammers are dispersed and are not concentrated in one area. Conventionally, this type of non-clustered deployment follows a uniform distribution. CJ, on the contrary, relates to a sort of jamming in which the jammers have close proximity, frequently forming groups or clusters. As a result of the clustered arrangement of jammers, it ends up in a limited and concentrated interfering pattern [8,9]. Conventionally, this type of deployment for clustered jammers follows the Matern cluster process (MCP).

MCP is a clustering point process that constitutes of parent and child nodes [10,11]. The jammers or child nodes are distributed around the cluster center or parent node in a specific radius following uniform distribution and the parent nodes do not participate in the overall point process [12,13]. In [14], a V2X network assisted by UAV is modeled with clustered jamming. The jammers are distributed using an MCP. The VNs consisting of vehicles, RSUs, and pedestrians are distributed using the Poisson line process (PLP), such that the VNs are assumed to reside along the roads (for details, see [15–17]). The UAVs are distributed randomly in the geographical region following the three-dimensional (3D) Poisson point process (PPP) (for details, see [18,19]). It was shown in [14] that the performance of the V2X networks is extremely degraded when MCP-distributed jammers are found in the neighborhood of VNs.

Some studies [20–22] focused on addressing jamming attacks on sink nodes positioned both within and outside clusters in wireless networks. The sink node, a crucial element in U-V2X communications, is responsible for transferring data from VNs to the network. It is essential to analyze jamming interference, particularly when the sink node is at the center

of a cluster and encounters jamming attacks from clustered jammers [23]. The sink node is typically positioned outside jamming clusters to enhance network performance in terms of capacity, connectivity, and reliability. However, when the sink node is at the center of a jamming cluster, enhancing the instantaneous received UL SIR at the typical node can improve the jamming interference. Reducing the number of jamming clusters and jammers per cluster can also enhance network performance. Additionally, increasing the size of the cluster representing the distribution of jammers in the geographical area and using narrow band frequency domain directional antennas with smaller beam width can further improve the negative effects of jamming in vehicular networks [24].

The importance of antenna beam width in controlling the jamming interference of wireless networks has been extensively studied in various research works [24–27]. Narrow beam width naturally limits the jamming area around the typical node, while wider beam width can be confined by improving the typical node's received SIR. Additionally, reducing the radius (or the size) of the cluster as well as the number of jamming clusters and jammers per cluster further confines the jamming area.

The path planning for UAVs with a focus on power and signal-to-noise ratio is explored in [28], using graphic- and heuristic-based algorithms to enhance UAV distance in anti-jamming environments. In [29], an anti-jamming power control scenario is proposed for UAV-assisted wireless networks, improving network performance in terms of sum rate and energy efficiency. For satellite-air-ground networks, [30] presents a two-stage scheme optimizing UAVs altitude and antenna beam-forming to address anti-jamming for Line-of-Sight links. Similarly, [31] considers the performance of aerial networks under Line-of-Sight links, optimizing jamming power control using a successive convex approximation technique. However, [28–31] did not provide insight into coverage and capacity performance for U-V2X communications.

Investigations into the data rate of typical user equipment in aerial terrestrial heterogeneous networks were conducted in [32]. The authors optimized the UAV trajectories and transmission power to enhance network performance. Additionally, they considered the impact of intentional jamming by smart jammers capable of tracking the UAVs. In [14], modeling the jamming interference in an aerial terrestrial heterogeneous network revealed that clustered ground jammers based on MCP degrade coverage and spectral efficiency (SE) performance. The work in [33] demonstrated compromised performance, particularly in probability of error, due to jamming signals in heterogeneous networks. The analysis in [34] addressed the aerial terrestrial heterogeneous networks with uniformly distributed jammers, focusing the crucial role of jammer height in characterizing jamming signals and their effect on outage probability (OP). However, the above-mentioned works are limited in the sense that they do not consider U-V2X communications.

1.2. Contributions and Organization

Typically, U-V2X networks encounter fluctuations in the 3D beam width of the antenna due to strong winds, high atmospheric pressure, mechanical noise, or error in the mechanical controllers. These fluctuations in the 3D beam width of the antenna can significantly reduce networks' performance. Recently, the authors in [35–37] modeled the fluctuations of the 3D beam width of the UAV antenna for mm-Waves. The authors showed that the system's performance is severely degraded with fluctuating beam width of the UAV and that it is very important to consider the antenna fluctuations for analyzing the realistic aerial network's performance. Thus, we investigate jamming in U-V2X networks for mm-Waves along with the UAV beam-width fluctuations. In the following ways, our work differs from recent related works:

- The work in [34] focused on jamming in aerial heterogeneous networks without considering UAV's fluctuating beam width and mm-Waves for vehicular communications. Moreover, this work focused on jamming in U-V2X communications by considering mm-Waves and UAV's fluctuating antenna beam width.

- The work in [35–37] focused on UAV's fluctuating 3D beam width with mm-Waves for aerial heterogeneous networks without focusing on U-V2X networks and jamming. Moreover, this work focused on UAV's fluctuating beam width with mm-Waves along with the jamming interference in U-V2X communications.
- The work in [14] explored C-V2X communications with micro-waves and jamming interference; this work specifically examined U-V2X communications with mm-Waves, taking into account both jamming interference and the fluctuating UAV beam width.
- The work in [9] concentrated on UAV beam-width fluctuations in U-V2X communications and their impact on success probability without considering jamming interference; this study focused on both jamming interference and UAV beam-width fluctuations in U-V2X communications, evaluating their impact on OP. Additionally, this research examined the effects of both non-clustered and clustered jammers on network performance. Furthermore, this work suggests prioritizing the implementation of anti-jamming techniques for non-clustered jammers with a higher probability rather than focusing solely on clustered jammers.

In all the aforementioned articles, analyzing the jamming of U-V2X communications along with the fluctuating beam width of the UAV is not considered, which can severely disrupt the networks' performance. Thus, in this article, we investigate the 3D beam width of the antenna fluctuations in U-V2X communications in the presence of jamming interference. The novel contributions of this article are as follows:

- The U-V2X system employing non-clustered and clustered jamming signals is presented, which faces disturbances owing to fluctuating 3D antenna beam width. Under this system, VNs communicate with adjacent VNs in their vicinity via a V2V connection or with UAVs via a V2U connection, taking into account characteristics such as network conditions, distance, and antenna strength.
- The analytical equations of the shortest distance and the probability of associations of the VNs with the surrounding VNs and UAVs are derived. By incorporating jammers along with the fluctuating antenna beam width, the derived equations provide a helpful understanding of the system's operation under a jamming environment.
- The analytical equations for the OP of V2V connection, VN to UAV connection (i.e., V2U2V), and U-V2X connection, considering both non-clustered and clustered jammers, are presented. The investigation also evaluates the impact of different setups for system effectiveness concerning OP and SE, such as the jammer's transmission power, average jammers, average UAVs, average VNs, and average roadways.
- The results illustrate that if challenged by impacts of non-clustered or clustered jammers along with 3D beam width of UAV antenna variations, the U-V2X system suffers significant operational deterioration. The findings suggested that anti-jamming countermeasures should be prioritized, specifically for non-clustered jammers in comparison with the clustered jammers. Furthermore, anti-jamming scenarios may reduce the negative impacts while improving the efficiency of U-V2X communications.
- The results further illustrate that at places with lesser vehicles, roads, and people; UAVs have a greater level of credibility in comparison with the VNs when it comes to setting up communication in intense jamming with non-clustered jammers. Additionally, it has been demonstrated that fewer variations in the beam width lead to more stable links provided by UAVs in U-V2X systems with jammers.

The paper is structured as follows: Section 2 describes the U-V2X system model, which takes into consideration non-clustered as well as clustered jammers, including UAV beam-width variations. The shortest path of a VN and adjoining UAV/VN is calculated in Section 3. Section 4 discusses the VN's AP in the presence of jammers, whereas Section 5 looks at the analysis of interference. Section 6 examines the VN's OP and SE. Section 7 offers the findings of the analysis and their implications, which leads to the conclusions in Section 8.

2. System Model

Our network for U-V2X communications under jamming interference consists of UAVs, VNs, and jammers as shown in Figure 2. UAVs were modeled according to a 3D PPP, Φ_U, with density, μ_U, and height, h_U. VNs were modeled on each road according to PLP, such that the roads follow PPP, Φ_L with the density of roads, λ_L, and the VNs are modeled on each road following 1D PPP, Φ_V, with density, μ_V, where $\mu_V = \mu_v + \mu_p + \lambda_{\mathbf{r}}$. μ_v indicates the density of vehicles in the area of interest, μ_p indicates the density of pedestrians in the area of interest, and $\mu_{\mathbf{r}}$ indicates the density of RSUs in the region-of-interest. The non-clustered jammer density is given by λ_J, where the jamming devices are scattered equally in the entire 2D space with radius, z. Conversely, the density of MCP-distributed jammers is given by $\lambda_J = \lambda_c \times J$, where λ_c is the density of parent nodes or cluster centers and J is the value of the number of jammers. The jamming devices are spread equally in a particular radius cluster, r_J. For a fair comparison of non-clustered jammers with clustered jammers, the total number of jammers' value is kept the same.

(**a**) Non-clustered jammers.

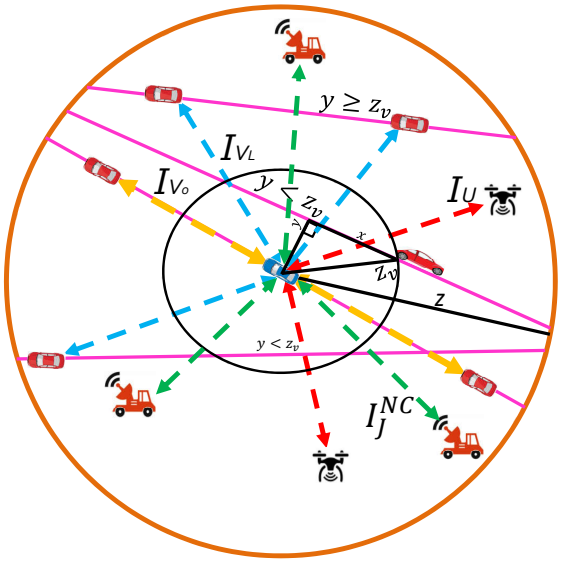

(**b**) Clustered jammers.

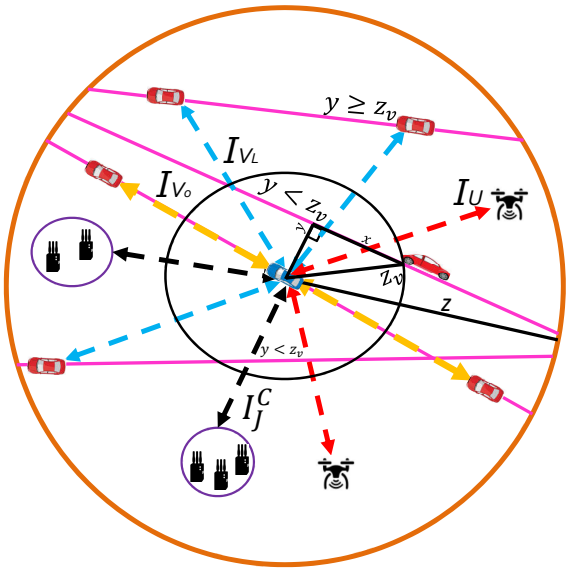

Figure 2. U-V2X system model with VNs, UAVs, and jammers.

P_W indicates the node's transmission power, where $W \in \{U, V\}$, such that P_U indicates the UAV's transmission power and it is assumed that UAVs do not have energy constraints and possess sufficient energy for communication purposes. The VN's transmit power is given by P_V and the jammer's transmit power is given by P_J. The path loss exponent associated with the UAV is given by α_U and the path loss associated with the VN is given by α_V. The path loss exponent associated with the jammers is given by α_J. The bias component is specified by $\mathcal{B}$, i.e., $\mathcal{B} = 0$ indicates that only UAVs are used by VNs and $\mathcal{B} = \infty$ indicates that VNs only utilize adjacent VNs for vehicular communications. The Rayleigh fading gain assumed between the channels of VNs and UAVs is given as g_W. For instance, g_U indicates the channel gain between the UAV, i.e., $g_U \sim \exp(1)$. Similarly, g_V is the channel gain between the VNs , i.e., $g_V \sim \exp(1)$.

The 3D gain of the $N_W \times N_W$ number of antenna is given as G_Q, i.e., $Q = \{t, r\}$, where t indicates a transmitting node and r indicates a receiving node. The deviation of the primary lobe of the antenna in the elevation and azimuth plane is given by θ and ϕ, respectively. The antenna gain can be defined by $G_Q = G_{Q,O} \times G_{Q,E}(N, \theta, \phi) \times G_{Q,A}(N, \theta, \phi)$, where $G_{Q,O}$ indicates the optimal gain along the primary beam width, $G_{Q,A}(N, \theta, \phi)$ indicates the gain of the antenna array factor, and $G_{Q,E}(\theta, \phi)$ indicates the gain of the individual antenna element.

By considering uniform amplitude, the excitation gain of the antenna array factor is given as follows:

$$G_{W,A}(N_W, \theta, \phi) = \left(\frac{\sin\left(\frac{N_W(\kappa_x \psi_x \sin(\theta)\cos(\phi) + \Delta_x)}{2} \right)}{N_W \sin\left(\frac{(\kappa_x \psi_x \sin(\theta)\cos(\phi) + \Delta_x)}{2} \right)} \times \frac{\sin\left(\frac{N_W(\kappa_y \psi_y \sin(\theta)\sin(\phi) + \Delta_y)}{2} \right)}{N_W \sin\left(\frac{(\kappa_y \psi_y \sin(\theta)\sin(\phi) + \Delta_y)}{2} \right)} \right)^2, \tag{1}$$

where $\kappa_x = \kappa_y$ is the wave number and is given by $2\pi f_c$, where f_c is the frequency. Moreover, the plate width and progressive phase shift for the x-axis are $\psi_x = c/2f_c$ and $\Delta_x = 0^\circ$, respectively, and for the y-axis are $\psi_y = c/2f_c$ and $\Delta_y = 0^\circ$, respectively, where c is the speed of light.

The gain of the single antenna element is defined as [38]:

$$G_{W,E}(\theta, \phi) = G_E^{\max} - \min\{-(G'(\theta_E) + G''(\theta_x)), \eta\}, \tag{2}$$

where $G' = -\min\left\{ -12\left(\frac{\theta_E - 90^\circ}{\mathcal{V}} \right)^2, \zeta \right\}$, $G'' = -\min\left\{ -12\left(\frac{\theta_E}{\mathcal{H}} \right)^2, \eta \right\}$, $\theta_E = \tan^{-1}\left(\sqrt{\frac{1 + \sin^2(\theta_x)}{\sin(\theta_y)}} \right)$, $G_E^{\max}$ is the highest gain, i.e., 8 dBi, $\mathcal{H}$ is the horizontal 3D beam width, i.e., 65°, $\mathcal{V}$ is the vertical 3D beam width, i.e., 65°, $\zeta = 30$ dB is the side-lobes limit, and $\eta = 30$ dB is the front-back ratio of antenna.

The transmission power with an equal and comparable outcome is given by Equation (2.22) of [39] as:

$$G_{W,0} = \frac{4\pi}{\int_0^{2\pi} \int_0^{\pi} G_{W,A}(N_W, \theta, \phi) \sin(\theta) d\theta d\phi}. \tag{3}$$

The path loss model for mm-Waves communications is not standardized yet, and thus, the path loss model defined by the 3GPP in [3] can be considered for a region with

building height, $h_b \leq 50$ m. The distance-dependent path loss at a distance, z, [dB] is defined as [36,37,40]:

$$Z(z) = 20\log_{10}\left(\frac{40\pi z f_c}{3}\right) + \min\left\{0.03h_b^{1.73}, 10\right\} \times \log_{10}(z) - \min\left\{0.044h_b^{1.73}, 14.77\right\} + 0.002z\log_{10}(h_b). \quad (4)$$

The uplink signal-to-interference ratio (SIR) can be computed as:

$$\mathrm{SIR}_t^r = \frac{P_t g_t G_t G_r \|z_r - z_t\|^{-\alpha_r}}{\sum_{i=1}^{I_n} P_t g_i G_{t,i} G_{r,i} \|z_r - z_i\|^{-\alpha_r} + \sum_{j=1}^{J_n} P_J g_j \|z_r - z_j\|^{-\alpha_J}}, \quad (5)$$

where the receiving/transmitting node is given as $\{r/t \in U, V\}$, the distance from the center of the coordinate plane to the transmitting node is given as z_t, the distance from the center of the coordinate plane to the receiving node is given as z_r, the distance from the center of the coordinate plane to the location of the i-th interferer is given as z_i, the number of interferers is given as I_n, the distance from the center of the coordinate plane to the location of the j-th jammer is given as z_j, and the number of jammers is given as J_n. Please note that the intended or serving signal from the sending node to the receiving node is declined from the interference analysis. Moreover, VN transmission utilizes F1 frequency and UAV transmission utilizes F2 frequency, such that, when VNs transmit, I_n indicates the maximum number of interfering VNs, and when UAVs transmit, I_n indicates the maximum number of interfering UAVs. Furthermore, this work highlights the communication of a VN with another VN either directly or through UAV. Thus, for for the direct V2V transmission, z_r is assumed to be at the center of the coordinate system, whereas for the V2U transmission, z_r is the distance from the center of the coordinate system to the UAV. Slivnyak's theorem states that by setting a single VN on a road at the coordinate system's center, the point process stays unaffected [15,41].

3. Distribution of Shortest Distance

3.1. Shortest Distance to a VN

The shortest distance for the communication of the VN with the nearest VN in V2V connection is defined according to the VN's shortest distance distribution to the nearby VN. The characterization of the shortest distance distribution of the VN with the nearest VN (referred by serving VN) located at a distance of z_V assumes that there is no other VN in its vicinity than the serving VN (i.e., the nearest VN), which can create an interfering signal stronger than the strength of the serving signal. The probability density function (PDF) of the distance to the VN is derived in Appendix A and is given as:

$$f_{z_V}(z_V) = \frac{dF_{z_V}(z_V)}{d_{z_V}} = 2\exp\left(-2\mu_V z_V + 2\pi\lambda_L \int_0^{z_V} 1 - e^{-2\mu_V\sqrt{z_V^2 - y^2}} dy\right)\left(\mu_V + 2\pi\lambda_L\mu_V \int_0^{z_V} \frac{z_V e^{-2\mu_V\sqrt{z_V^2-y^2}}}{\sqrt{z_V^2 - y^2}} dy\right). \quad (6)$$

3.2. Shortest Distance to a UAV

The shortest distance for the communication of the VN with the closest UAV connection is characterized by the shortest distance distribution of the VN to the UAV. The characterization of the shortest distance distribution of the VN with the closest UAV (referred to as a serving UAV) positioned at a distance of z_U assumes that no other UAV resides in a spherical shape of the radius, z_U, from the serving UAV (i.e., the closest UAV),

which can create an interfering signal stronger than the serving signal's strength. This PDF distance is expressed by [15,42]:

$$f_{z_U}(z_U) = 2\pi\mu_U \exp\left(-\pi\mu_U z_U^2\right). \tag{7}$$

4. Association Probability of the VN with a Nearby UAV and VN

VNs can communicate with other VNs by associating with adjacent UAVs or other VNs. The association of the VN with the adjacent VN or UAV is characterized in terms of the AP. Typically, the AP of the VN with another VN or UAV is governed by the received strength at the VN or UAV.

4.1. V2V Connection's AP

The probability that the VN will associate itself with the adjacent VN based on the received power at the adjacent VN is referred to as a V2V connection's AP. Conventionally, when the power that is obtained by the VN from the closest VN exceeds the power obtained by the closest UAV, VN associates itself with the closest VN. The likelihood of association of the VN with the adjacent VN is referred to as the AP of the VN and is given as:

$$\mathbf{A}_V = \int_0^\infty \Pr\{\mathcal{A}_V(V2V \setminus z_V)\} f_{z_V}(z_V) dz_V, \tag{8}$$

where the probability of association of the VN with the adjacent VN, $\mathcal{A}_V(V2V \setminus z_V)$ is computed under the assumption that there is not any other VN located within a spherical shape of the radius, z_V, from the coordinate system's center. The AP of the VN is derived as:

$$\begin{aligned}
\Pr\{\mathcal{A}_V(V2V \setminus z_V)\} &= \Pr\left\{\mathcal{B}\, z_V^{-\alpha_V} G_{r,V} > z_U^{-\alpha_U} G_{r,U}\right\} \\
&= \Pr\left\{\frac{\mathcal{B}\, z_V^{-\alpha_V} G_{r,V}}{G_{r,U}} > z_U^{-\alpha_U}\right\} \\
&= \Pr\left\{z_U > \left(\frac{z_V^{\alpha_V} G_{r,U}}{\mathcal{B}\, G_{r,V}}\right)^{1/\alpha_U}\right\}.
\end{aligned} \tag{9}$$

We may construct the subsequent equation by replacing the complementary cumulative distribution function (CCDF) for z_U into (9), which is given as:

$$\Pr\{\mathcal{A}_V(V2V \setminus z_V)\} = \exp\left(-\pi\mu_U \left(\left(\frac{z_V^{\alpha_V} G_{r,U}}{\mathcal{B}\, G_{r,V}}\right)^{1/\alpha_U}\right)^2\right). \tag{10}$$

VNs may increase the gain by aligning their antennas since they are not bound by issues such as battery limits or payload restraints. As a result, (10) may be reduced to $G_{r,0}(N_V) = G_{r,V}(N_V, \theta, \phi)$. We can calculate the AP of the V2V link by inserting (10) and (6) into (8). The final expression is as follows:

$$\begin{aligned}
\mathbf{A}_V = \int_0^\infty 2\exp\left(-\pi\mu_U \left(\left(\frac{z_V^{\alpha_V} G_{r,U}}{\mathcal{B}\, G_{r,0}}\right)^{1/\alpha_U}\right)^2\right) \\
\exp\left(-2\mu_V z_V + 2\pi\lambda_L \int_0^{z_V} 1 - e^{-2\mu_V\sqrt{z_V^2 - y^2}} dy\right)\left(\mu_V + 2\pi\lambda_L\mu_V \int_0^{z_V} \frac{z_V e^{-2\mu_V\sqrt{z_V^2-y^2}}}{\sqrt{z_V^2 - y^2}} dy\right) dz_V.
\end{aligned} \tag{11}$$

4.2. V2U Connection's AP

The probability that the VN will associate itself with the adjacent UAV based on its received power at the UAV is referred to as a V2U connection's AP. Conventionally, when the power that is obtained by the VN from the closest VN is lower the power obtained by the closest UAV, VN associates itself with the UAV. The likelihood of association of the VN with the UAV is referred to as the AP of the UAV and is given as:

$$\mathbf{A}_U = \int_0^\infty \Pr\{\mathcal{A}_U(V2U \setminus z_U)\} f_{z_U}(z_U) d_{z_U}, \tag{12}$$

where AP of VN with UAV assuming no other UAV in the given region can be expressed by $\mathcal{A}_U(V2U \setminus z_U)$. The AP of the UAV is derived as:

$$\begin{aligned}\Pr\{\mathcal{A}_U(V2U \setminus z_U)\} &= \Pr\left\{ z_U^{-\alpha_U} G_{r,U} > \mathcal{B}\, z_V^{-\alpha_V} G_{r,V} \right\} \\ &= \Pr\left\{ \frac{z_U^{-\alpha_U} G_{r,U}}{\mathcal{B}\, G_{r,V}} > z_V^{-\alpha_V} \right\} \\ &= \Pr\left\{ z_V > \left(\frac{\mathcal{B}\, z_U^{\alpha_U} G_{r,V}}{G_{r,U}} \right)^{1/\alpha_V} \right\}. \end{aligned} \tag{13}$$

We may construct the subsequent equation by replacing the CCDF for z_V into (13) to obtain the resultant equation as:

$$\begin{aligned}\Pr\{\mathcal{A}_U(V2U \setminus z_U)\} = \exp\Bigg(-2\pi\lambda_L \int_0^{\left(\mathcal{B}\, z_U^{\alpha_U} G_{r,O}/G_{r,U}\right)^{1/\alpha_V}} \\ \left(1 - e^{-2\mu_V \sqrt{\left(\left(\mathcal{B}\, z_U^{\alpha_U} G_{r,0}/G_{r,U}\right)^{1/\alpha_V}\right)^2 - y^2}} \right) dy \Bigg) \exp\left(-2\mu_V \left(\left(\mathcal{B}\, z_U^{\alpha_U} G_{r,0}/G_{r,U}\right)^{1/\alpha_V} \right)^2 \right). \end{aligned} \tag{14}$$

The $\mathbf{A}_U$ equation may be obtained by replacing (14) and the PDF of z_U in (12) as:

$$\begin{aligned}\mathbf{A}_U = \int_0^\infty \exp\Bigg(-2\pi\lambda_L \int_0^{\left(\mathcal{B}\, z_U^{\alpha_U} G_{r,0}/G_{r,U}\right)^{1/\alpha_V}} \left(1 - e^{-2\mu_V \sqrt{\left(\left(\mathcal{B}\, z_U^{\alpha_U} G_{r,0}/G_{r,U}\right)^{1/\alpha_V}\right)^2 - y^2}} \right) dy \Bigg) \\ \exp\left(-2\mu_V \left(\left(\mathcal{B}\, z_U^{\alpha_U} G_{r,0}/G_{r,U}\right)^{1/\alpha_V} \right)^2 \right) 2\pi\mu_U z_U \exp\left(-\pi\mu_U z_U^2 \right) dz_U. \end{aligned} \tag{15}$$

5. Interference Classification

This section examines the interference produced by UAVs, VNs, and non-clustered or clustered jammers. To investigate VN-UAV interference, the Laplace transform is used, which allows the system's performance metrics such as OP and SE to be effectively calculated.

5.1. VN's Interference

5.1.1. Interference of the VNs (From the Roads Avoiding Center of the Coordinate System)

The VNs' interference can be expressed as $L_{I_{z_r}}(s) = \mathbb{E}[\exp(-s\, I)]$, where $I = \sum_{i \in I_{z_r}} P_t g_i G_{t,i} G_{r,i} \| z_r - z_i \|^{-\alpha_r}$ and $s = \| z_r - z_t \|^{\alpha_r} \tau / P_t$. The interference is given by:

$$L_{I_{z_r}}(s \setminus z_r) = \mathbb{E}_{g,z}\left[\prod_{i\in I_{z_r}} \exp\left(-sP_t g_i G_{t,i} G_{r,i} \|z_r - z_i\|^{-\alpha_r}\right)\right]$$
$$\stackrel{1}{=} \mathbb{E}_z\left[\prod_{i\in I_{z_r}} \mathbb{E}_g\left[\exp\left(-sP_t g_i G_{t,i} G_{r,i} \|z_r - z_i\|^{-\alpha_r}\right)\right]\right]$$
$$\stackrel{2}{=} \mathbb{E}_z\left[\prod_{i\in I_{z_r}} \frac{1}{1 + sP_r G_{t,i} G_{r,i} \|z_r - z_i\|^{-\alpha_r}}\right]. \quad (16)$$

where (1) is obtained by assuming independent point process and (2) is derived as a result of exponentially distributed fading gain with unity mean power.

To account for the interference of the VNs resulting from just one road crossing a spherical shape, $\mathbf{S}(0, z_V)$, we compute two independent Laplace equations. They are represented by $L'_{I_V}(s \setminus z)$ (for VNs on roads that intersect the specified territory, such that $y < z_V$) and $L''_{I_V}(s \setminus z)$ (for VNs on roadways which are not traversing the area, i.e., $y \geq z_V$). This variation is due to the various geographical arrangements of VNs along these roadways. VNs on crossing roadways have been placed on a line segment between $\left[-\sqrt{z^2 - y^2}, -\sqrt{z_V^2 - y^2}\right]$ and $\left[\sqrt{z_V^2 - y^2}, \sqrt{z^2 - y^2}\right]$. VNs located on non-intersecting roadways, on the other hand, are discovered on a line segment between $\left[-\sqrt{z^2 - y^2}, 0\right]$ and $\left[0, \sqrt{z^2 - y^2}\right]$. The interference associated with VNs is assessed using these various geographical configurations as $L'_{I_V}(s \setminus z)$ and $L''_{I_V}(s \setminus z)$, respectively.

Assuming a is the distance that separates two VNs on a path (i.e., a line segment). The VNs' interference without crossing a spherical form provided by $\mathbf{S}(0, z_V)$ is obtained by assuming that each VN on a highway has a probability of m and assuming the specified path has a homogeneous distribution with PDF, $f(a) = 1/2\sqrt{z^2 - y^2}$. The receiving site signal interruption is therefore described as:

$$L''_{I_V}(s \setminus z) = \sum_{m\geq 0} \Pr\{N_V = m\} \int_{-\sqrt{z^2-y^2}}^{\sqrt{z^2-y^2}} \left(f(a)/1 + sP_V G_t G_r \left(y^2 + a^2\right)^{\frac{-\alpha_V}{2}}\right)^m. \quad (17)$$

Utilizing PPP's probability of uniformly distributed points and then plugging $f(a)$ in (17), we obtain:

$$L''_{I_V}(s \setminus z) = \sum_{m\geq 0} \frac{e^{\left(-2\mu_V\sqrt{z^2-y^2}\right)}\left(2\mu_V\sqrt{z^2-y^2}\right)^m}{m!\left(2\sqrt{z^2-y^2}\right)^m} \left(\int_{-\sqrt{z^2-y^2}}^{\sqrt{z^2-y^2}} da/1 + sP_V G_t G_r \left(y^2 + a^2\right)^{\frac{-\alpha_V}{2}}\right)^m.$$

Assuming $\sum_{m=0}^{\infty} \frac{\mathcal{Y}^m}{m!} = e^{\mathcal{Y}}$ and $\int_{-a}^{a} = 2a$, the equation is given as:

$$L''_{I_V}(s \setminus z) = e^{\left(-2\mu_V\sqrt{z^2-y^2}\right)} \exp\left(2\mu_V \left(\int_0^{\sqrt{z^2-y^2}} da/1 + sP_V G_t G_r \left(y^2 + a^2\right)^{\frac{-\alpha_V}{2}}\right)\right).$$

Simple mathematical operations offer the formula for single road's interference, $y \geq z_V$, which is represented as:

$$L''_{I_V}(s \setminus z) = \exp\left(-2\mu_V \int_0^{\sqrt{z^2-y^2}} \left(1 - \frac{1}{1 + sP_V G_t G_r (y^2 + a^2)^{\frac{-\alpha_V}{2}}}\right) da\right).$$

Assuming $\alpha_V > 1$, the closed-form solution is:

$$L''_{I_V}(s \setminus z) = \exp\left(-2\mu\pi(sP_V G_t G_r)^{-\alpha_V} \csc\left(\frac{\pi}{\alpha_V}\right)/\alpha_V\right). \tag{18}$$

In the same way, interference of the VNs with $y < z_V$, might be determined and represented as:

$$L'_{I_V}(s \setminus z) = \exp\left(-2\mu_V \int_{\sqrt{z_V^2 - y^2}}^{\sqrt{z^2 - y^2}} \left(1 - \frac{1}{1 + sP_V G_t G_r (y^2 + a^2)^{\frac{-\alpha_V}{2}}}\right) da\right).$$

For $\alpha_V = 3$, the closed-form solution with $z > 0$ is expressed by:

$$L'_{I_V}(s \setminus z) = \exp\left(\frac{2\mu_V}{3(sP_V G_t G_r)^{-1/3}}\left\{-\log(z) + \log\left(z + (sP_V G_t G_r)^{1/3}\right)\right.\right.$$
$$\left.\left. + (-1)^{2/3}\log\left(1 + \frac{(-1)^{2/3}}{z(sP_V G_t G_r)^{-1/3}}\right) - (-1)^{1/3}\log\left(1 - \frac{(-1)^{1/3}}{z(sP_V G_t G_r)^{-1/3}}\right)\right\}\right) \tag{19}$$

The interference expression is obtained for each highway crossing $\mathbf{S}(o, z_V)$ by establishing that the likelihood of roadways crossing $\mathbf{S}(o, z_V)$ is a PPP with an average of $2\lambda_L\mu_V(z - z_V)$. Furthermore, the mean value of highways in $\mathbf{S}(o, z)$ that do not intersect with $\mathbf{S}(o, z_V)$ constitutes a PPP with average highways in the physical area of interest supplied as $2\lambda_L\mu_V z$. Assume k_1 and k_2 represent the number of highways in the defined region, with k_1 taking the PDF, $f(b_1) = 1/2z$ with $y \geq z$, and k_2 taking the PDF, $f(b_2) = 1/2(z - z_V)$ with $y < z$. The interference of highways other than the ones passing the site of the center of the coordinate system is characterized as:

$$L_{I_V}(s \setminus z) = \left\{\sum_{k_1 \geq 0} \frac{\exp(-2\lambda_L\mu_V z)(2\lambda_L\mu_V z)^{k_1}}{k_1!}\left(\int_{-z}^{z} L''_{I_V}(s \setminus z) f(b_1) db_1\right)^{k_1}\right\}$$
$$\left\{\sum_{k_2 \geq 0} \frac{\exp(-2\lambda_L\mu_V (z - z_V))(2\lambda_L\mu_V (z - z_V))^{k_2}}{k_2!}\left(\int_{z_V}^{z} L'_{I_V}(s \setminus z) f(b_2) db_2\right)^{k_2}\right\}. \tag{20}$$

The equation may be simplified by putting $f(b_1)$ and $f(b_2)$ into (20) and using basic mathematical tools, and is given as:

$$L_{I_V}(s \setminus z) = \exp(-2\lambda_L\mu_V z)\frac{\sum_{k_1 \geq 0}\left(2\lambda_L\mu_V \int_0^z L''_{I_V}(s \setminus z) db_1\right)^{k_1}}{k_1!}$$
$$\exp(-2\lambda_L\mu_V (z - z_V))\frac{\sum_{k_2 \geq 0}\left(2\lambda_L\mu_V \int_{z_V}^{z} L'_{I_V}(s \setminus z) db_2\right)^{k_2}}{k_2!}. \tag{21}$$

Following $\sum_{i=0}^{\infty} \mathcal{Y}^i/i! = e^{\mathcal{Y}}$, (21) is expressed as:

$$L_{I_V}(s \setminus z) = \exp(-2\lambda_L\mu_V z)\exp\left(2\lambda_L\mu_V \int_0^z L''_{I_V}(s \setminus z) db_1\right)$$
$$\exp(-2\lambda_L\mu_V (z - z_V))\exp\left(2\lambda_L\mu_V \int_{z_V}^{z} L'_{I_V}(s \setminus z) db_2\right). \tag{22}$$

Lastly, the interference of the VNs across every highway, except the one passing via the center of the coordinate system, is provided by:

$$L_{I_V}(s \setminus z) = \exp\left(-2\lambda_L \mu_V \int_0^z \left(1 - L''_{I_V}(s \setminus z)\right) db_1 + \int_{z_V}^z \left(1 - L'_{I_V}(s \setminus z)\right) db_2\right). \quad (23)$$

5.1.2. Interference of the VNs (From the Roads Passing Origin)

The VNs' interference from a road traversing the center of the coordinate system is accomplished by following the assumption $y = 0$ in (19) and being expressed as:

$$L_{I_{V_o}}(s \setminus z) = \exp\left(-2\mu_V \int_{z_V}^z \left(1 - \frac{1}{1 + sP_V G_t G_r b^{-\alpha_V}}\right) db\right). \quad (24)$$

The closed-form with $\alpha_V > 1$, $z_V \approx 0$, and $z > 0$ is given as:

$$L_{I_{V_o}}(s \setminus z = \exp\left(\frac{-2\mu_V G_t G_r z \; {}_2F_1\left(1, \frac{-1+\alpha_V}{\alpha_V}; 2 - \frac{1}{\alpha_V}; -G_t G_r z\right)}{1 + \alpha_V}\right), \quad (25)$$

where ${}_2F_1(-,-;-;-)$ is the hyper-geometric function [43].

5.2. UAV's Interference

UAV interference refers to the interfering signals from the adjacent UAVs during U2V communication. This form of interference is characterized by $L_{I_U}(s) = \mathbb{E}[\exp(-sI_U)]$, where I_U indicates the UAVs' interference. The UAV interference is given as [42]:

$$\begin{aligned} L_{I_U}(s \setminus z) &= \mathbb{E}[\exp(-s\ I_U)] \\ &\stackrel{1}{=} \exp\left(-2\pi\mu_U \int_{z_U}^z (1 - \mathbb{E}\left[\exp\left(sP_U g_U G_t G_r b^{-\alpha_U}\right)\right]) b\ db\right) \\ &\stackrel{2}{=} \exp\left(-2\pi\mu_U \int_{z_U}^z \left(1 - \frac{1}{1 + sP_U G_t G_r b^{-\alpha_U}}\right) b\ db\right). \end{aligned} \quad (26)$$

where (1) is obtained assuming polar coordinates and applying the probability-generating function of PPP and (2) is obtained by supposing g_U to be exponentially distributed with the mean of unity.

5.3. Jammer's Interference

The non-clustered/clustered jammers' interference can be described in the context of the Laplace transform of interference, $L_{I_J}(s)$.

5.3.1. Non-Clustered Jamming

Jamming intrusion from jamming devices substantially disrupts the legal U-V2X transmission. For non-clustered jammers, jamming devices can be distributed according to the uniform distribution in the given region's radius, z. Appendix B describes the interference of uniformly dispersed jammers. and is expressed as:

$$\begin{aligned} L_{I_J^{NC}}(\tau) = \exp\Bigg\{ & \frac{2\pi\Delta\lambda_J \tau z_1^{2-\alpha_r}}{z^{-\alpha_r}(\alpha_r - 2)} \\ & {}_2F_1\left(1, 1 - \frac{2}{\alpha_r}; 2 - \frac{2}{\alpha_r}; -\Delta\tau\left(\frac{z}{z_1}\right)^{\alpha_r}\right) - \frac{2\pi\Delta\lambda_J \tau z_0^{2-\alpha_r}}{z^{-\alpha_r}(\alpha_r - 2)} {}_2F_1\left(1, 1 - \frac{2}{\alpha_r}; 2 - \frac{2}{\alpha_r}; -\Delta\tau\left(\frac{z}{z_0}\right)^{\alpha_r}\right)\Bigg\}. \end{aligned} \quad (27)$$

5.3.2. Clustered Jamming

When the number of jammers, J, are distributed around the cluster center with density, λ_c, in a circular region of the radius, r_J, according to an MCP, the jamming interference at the receiving node is derived in Appendix C and is expressed as: [14]

$$L_{I_J^C}(\tau) = \exp\left\{-\frac{2\pi\lambda_c J}{\alpha_r r_J^2}\tau^{2/\alpha_r}\csc\left(\frac{2\pi}{\alpha_r}\right)z^2 - \pi\lambda_c\tau^{2/\alpha_r}z^2\int_0^z\left(1-\exp\left(\frac{-J}{1+\omega^{\alpha_r/2}}\right)\right)d\omega\right\}. \quad (28)$$

6. Performance Metrics

6.1. OP Performance

The OP is characterized as the probability that the recipient node's instantaneous SIR is less than a pre-established threshold value, τ. The OP for a receiving node to be less than the coverage threshold is expressed as follows:

$$\mathcal{O}_t^r = \int_0^\infty \Pr\{\mathrm{SIR}_t^r \le \tau\} f_{z_{t2r}}(z_{t2r}) dz_{t2r} \quad (29)$$

where the PDF distance corresponding to the gap that separates the sending and receiving nodes is given as $f_{z_{t2r}}(z_{t2r})$. The OP of the receiving node can also be determined by the chance to be in coverage and is given as:

$$\mathcal{O}_t^r = \int_0^\infty (1-\Pr\{\mathrm{SIR}_t^r > \tau\}) f_{z_{t2r}}(z_{t2r}) dz_{t2r} = \int_0^\infty (1-\mathcal{C}_t^r) f_{z_{t2r}}(z_{t2r}) dz_{t2r}, \quad (30)$$

where $\mathcal{C}_t^r$ indicates the coverage of the receiving node. Thus, V2V's OP is stated as:

$$\mathcal{O}_V^V = \int_0^\infty \left(1-\mathcal{C}_V^V\right) f_{z_{V2V}}(z_{V2V}) dz_{V2V} \quad (31)$$

The coverage of the V2V connection (i.e., $\mathcal{C}_V^V$) assumes that the VN is connected to the nearest VN and that no other VN resides in a spherical shape of the radius, z_V, around it. Moreover, for the connection to be in an outage, the obtained SIR must be below the threshold value. The PDF distance of VN-VN is expressed as $f_{z_{V2V}}(z_{V2V})$. Furthermore, by introducing jamming into the system, the resulting expression for (31) is described below:

$$\mathcal{O}_{J_V^V} = \int_0^\infty 1 - L_{I_V}(s \setminus z_{V2V}) L_{I_{V_o}}(s \setminus z_{V2V}) L_{I_J}(s \setminus z_{V2U}) f_{z_{V2V}}(z_{V2V}) dz_{V2V}. \quad (32)$$

The probability of outage for the V2V connection with uniformly distributed jammers is obtained in (33) by inserting (23), (24), (27), and (6) into (32) and assuming network settings as $z_{V2V} = z_V$, $r = V$, and $s = \tau P_V^{-1} z_V^{\alpha_V}$. Similarly, the probability of outage for the V2V connection with MCP-distributed jammers is obtained in (34) by inserting (23), (24), (28), and (6) into (32) and assuming network settings as $z_{V2V} = z_V$, $r = V$, and $s = \tau P_V^{-1} z_V^{\alpha_V}$. Note that (34) gives a reference graph for the OP of a LB on V2V curve and analyzes the OP if transmission between VNs and neighboring VNs occurs via just VNs (i.e., 100% affiliation to VNs while ignoring UAVs):

$$
\begin{aligned}
&\mathcal{O}_{NC_V^V} = \int_0^{\infty} 1 - \exp\left(-2\lambda_L \mu_V \int_0^{z} \left(1 - L''_{I_V}\right) db_1 + \int_{z_V}^{z} \left(1 - L'_{I_V}\right) db_2\right) \\
&\exp\left(-2\mu_V \int_0^{z} \left(1 - \frac{1}{1 + \tau z_V^{\alpha_V} G_t G_r b^{-\alpha_V}}\right) db\right) \\
&\exp\left\{\frac{2\pi\Delta\lambda_J \tau z_1^{2-\alpha_V}}{z_V^{-\alpha_V}(\alpha_V - 2)} {}_2F_1\left(1, 1 - \frac{2}{\alpha_V}; 2 - \frac{2}{\alpha_V}; -\Delta\tau\left(\frac{z_V}{z_1}\right)^{\alpha_V}\right) - \right. \\
&\left. \frac{2\pi\Delta\lambda_J \tau z_0^{2-\alpha_V}}{z_V^{-\alpha_V}(\alpha_V - 2)} {}_2F_1\left(1, 1 - \frac{2}{\alpha_V}; 2 - \frac{2}{\alpha_V}; -\Delta\tau\left(\frac{z_V}{z_0}\right)^{\alpha_V}\right)\right\} \\
&2\exp\left(-2\mu_V z_V + 2\pi\lambda_L \int_0^{z_V} 1 - e^{-2\mu_V \sqrt{z_V^2 - y^2}} dy\right) \left(\mu_V + 2\pi\lambda_L \mu_V \int_0^{z_V} \frac{z_V e^{-2\mu_V \sqrt{z_V^2 - y^2}}}{\sqrt{z_V^2 - y^2}} dy\right) dz_V.
\end{aligned}
\tag{33}
$$

$$
\begin{aligned}
&\mathcal{O}_{C_V^V} = \int_0^{\infty} 1 - \exp\left(-2\lambda_L \mu_V \int_0^{z} \left(1 - L''_{I_V}\right) db_1 + \int_{z_V}^{z} \left(1 - L'_{I_V}\right) db_2\right) \\
&\exp\left(-2\mu_V \int_0^{z} \left(1 - \frac{1}{1 + \tau z_V^{\alpha_V} G_t G_r b^{-\alpha_V}}\right) db\right) \\
&\exp\left\{-\frac{2\pi\lambda_c J}{\alpha_V r_J^2} \tau^{2/\alpha_V} \csc\left(\frac{2\pi}{\alpha_V}\right) z_V^2 - \pi\lambda_c \tau^{2/\alpha_V} z_V^2 \int_0^{\infty} \left(1 - \exp\left(\frac{-J}{1 + \omega^{\alpha_V/2}}\right)\right) d\omega\right\} \\
&2\exp\left(-2\mu_V z_V + 2\pi\lambda_L \int_0^{z_V} 1 - e^{-2\mu_V \sqrt{z_V^2 - y^2}} dy\right) \left(\mu_V + 2\pi\lambda_L \mu_V \int_0^{z_V} \frac{z_V e^{-2\mu_V \sqrt{z_V^2 - y^2}}}{\sqrt{z_V^2 - y^2}} dy\right) dz_V.
\end{aligned}
\tag{34}
$$

In a setting wherein communication occurs through UAVs, the OP of the V2V link is provided by:

$$
\mathcal{O}^{V2V} = \mathbf{A}_V \mathcal{O}_V^V. \tag{35}
$$

The V2U's OP can be described as the probability that the SIR at the UAV is less than the pre-set threshold value. The V2U's OP has been determined assuming the minimal transmission and reception distance of the VN and the UAV is z_{V2U}. The OP of the V2U link is determined by:

$$
\mathcal{O}_V^U = \int_0^{\infty} \left(1 - \Pr\{\mathrm{SIR}_V^U > \tau\}\right) f_{z_{V2U}}(z_{V2U}) dz_{V2U} = \int_0^{\infty} \left(1 - \mathcal{C}_V^U\right) f_{z_{V2U}}(z_{V2U}) dz_{V2U}, \tag{36}
$$

where the coverage of the V2U link is given by $\mathcal{C}_V^U$ and the PDF distance of the VN to UAV link is given by $f_{z_{V2U}}(z_{V2U})$. The expression for the OP of the V2U link with jamming is given by:

$$
\mathcal{O}_{J_V^U} = \int_0^{\infty} 1 - L_{I_V}(s \setminus z_{V2U}) L_{I_{V_o}}(s \setminus z_{V2U}) L_{I_J}(s \setminus z_{V2U}) f_{z_{V2U}}(z_{V2U}) dz_{V2U}. \tag{37}
$$

Plugging (23), (24), (28), and (6) in (37), considering network settings as $z_{V2U} = z_U$, $r = U$, and $s = \tau P_V^{-1} z_U^{\alpha_U}$, and assuming MCP-distributed jammers, the formula that accounts for the effectiveness of the V2U link is determined and presented in (39). In a similar way, plug (23), (24), (27), and (6) in (37), considering network settings as $z_{V2U} = z_U$, $r = U$, and $s = \tau P_V^{-1} z_U^{\alpha_U}$, and assuming uniformly distributed jammers, the formula that accounts for the effectiveness of the V2U link with uniformly distributed jammers is determined and presented in (38). It must be mentioned that (39) and (38) might be used when only UAVs are authorized to send information from sending VN to the recipient VN. Furthermore, (39) gives a reference graph for the OP of LB on V2U2V graph and analyzes

the OP during the interaction between UAVs along with recipient VNs (i.e., 100% affiliation of VNs to the UAVs):

$$\begin{aligned}
&\mathcal{O}_{NC_V^U} = \int_0^{\infty} 1 - \exp\left(-2\lambda_L\mu_V\int_0^{z}\left(1 - L''_{I_V}\right)db_1 + \int_{z_U}^{z}\left(1 - L'_{I_V}\right)db_2\right)\\
&\exp\left(-2\mu_V\int_0^{z}\left(1 - \frac{1}{1+\tau z_U^{\alpha_U} G_t G_r b^{-\alpha_U}}\right)db\right)\\
&\exp\left\{\frac{2\pi\Delta\lambda_J\tau z_1^{2-\alpha_U}}{z_U^{-\alpha_U}(\alpha_U-2)}{}_2F_1\left(1, 1-\frac{2}{\alpha_U}; 2-\frac{2}{\alpha_U}; -\Delta\tau\left(\frac{z_U}{z_1}\right)^{\alpha_U}\right) - \right.\\
&\left.\frac{2\pi\Delta\lambda_J\tau z_0^{2-\alpha_U}}{z_U^{-\alpha_U}(\alpha_U-2)}{}_2F_1\left(1, 1-\frac{2}{\alpha_U}; 2-\frac{2}{\alpha_U}; -\Delta\tau\left(\frac{z_U}{z_0}\right)^{\alpha_U}\right)\right\}\\
&2\exp\left(-2\mu_V z_U + 2\pi\lambda_L\int_0^{z_U} 1 - e^{-2\mu_V\sqrt{z_U^2-y^2}}dy\right)\left(\mu_V + 2\pi\lambda_L\mu_V\int_0^{z_U}\frac{z_U e^{-2\mu_V\sqrt{z_U^2-y^2}}}{\sqrt{z_U^2-y^2}}dy\right)dz_U.
\end{aligned} \tag{38}$$

$$\begin{aligned}
&\mathcal{O}_{C_V^U} = \int_0^{\infty} 1 - \exp\left(-2\lambda_L\mu_V\int_0^{z}\left(1 - L''_{I_V}\right)db_1 + \int_{z_U}^{z}\left(1 - L'_{I_V}\right)db_2\right)\\
&\exp\left(-2\mu_V\int_0^{z}\left(1 - \frac{1}{1+\tau z_U^{\alpha_U} G_t G_r b^{-\alpha_U}}\right)db\right)\\
&\exp\left\{-\frac{2\pi\lambda_c J}{\alpha_U r_f^2}\tau^{2/\alpha_U}\csc\left(\frac{2\pi}{\alpha_U}\right)z_U^2 - \pi\lambda_c\tau^{2/\alpha_U}z_U^2\int_0^{\infty}\left(1 - \exp\left(\frac{-J}{1+\omega^{\alpha_U/2}}\right)\right)d\omega\right\}\\
&2\exp\left(-2\mu_V z_U + 2\pi\lambda_L\int_0^{z_U} 1 - e^{-2\mu_V\sqrt{z_U^2-y^2}}dy\right)\left(\mu_V + 2\pi\lambda_L\mu_V\int_0^{z_U}\frac{z_U e^{-2\mu_V\sqrt{z_U^2-y^2}}}{\sqrt{z_U^2-y^2}}dy\right)dz_U.
\end{aligned} \tag{39}$$

The OP of the U2V connection is defined as the possibility of achieving an SIR lesser than the pre-set limit, τ. The OP for the U2V connection that corresponds to the closest distance, z_{U2V}, between the sending UAV and the target VN is provided as:

$$\mathcal{O}_U^V = \int_0^{\infty}\left(1 - \Pr\{\mathrm{SIR}_U^V > \tau\}\right)f_{z_{U2V}}(z_{U2V})dz_{U2V} = \int_0^{\infty}\left(1 - \mathcal{C}_U^V\right)f_{z_{U2V}}(z_{U2V})dz_{U2V} \tag{40}$$

The PDF between the transmitting UAV and the receiver's VN at the center of the coordinate system is given by $f_{z_{U2V}}(z_{U2V})$ and the coverage of the U2V connection is given by $\mathcal{C}_U^V$. The OP of the U2V connection is expressed as:

$$\mathcal{O}_U^V = \int_0^{\infty} 1 - L_{I_U}(s \setminus z_{U2V})f_{z_{U2V}}(z_{U2V})dz_{U2V}. \tag{41}$$

The U2V connection's OP is obtained in (42) by plugging (7) and (26) in (41) and considering network settings as $z_{U2V} = z_U$ and $s = \tau P_U^{-1} z_U^{\alpha_U}$:

$$\mathcal{O}_U^V = \int_0^{\infty}\exp\left(-2\pi\mu_U\int_{z_U}^{z}\left(\left(1 - \frac{1}{1+\tau z_U^{-\alpha_U} G_t G_r b^{-\alpha_U}}\right)b\right)db\right)2\pi\mu_U\exp\left(-\pi\mu_U z_U^2\right)dz_U. \tag{42}$$

The V2U2V connection is a hybrid link that supports both V2V and U2V transmissions. The OP of the V2U2V connection is stated as:

$$\mathcal{O}^{V2U2V} = \mathbf{A}_U\mathcal{O}_V^U\mathcal{O}_U^V. \tag{43}$$

The V2U2V's analytical equation with uniformly distributed jammers is obtained by plugging (15), (38), and (42) in (43). Similarly, the V2U2V's analytical equation with MCP-distributed jammers is obtained by plugging (15), (39), and (42) in (43). The V2V and

V2U2V links are joined in the U-V2X connection. The OP of the U-V2X connection is as follows:

$$\begin{aligned}\mathcal{O}^{U-V2X} &= \mathcal{O}^{V2V} + \mathcal{O}^{V2U2V} \\ &= \mathbf{A}_V \mathcal{O}_V^V + \mathbf{A}_U \mathcal{O}_V^U \mathcal{O}_U^V. \end{aligned} \tag{44}$$

The final equation of the U-V2X connection with uniformly distributed jammers is produced by plugging (11), (33), (15), (38), and (42) in (44). Similarly, the final equation of the U-V2X connection with MCP-distributed jammers is produced by plugging (11), (34), (15), (39), and (42) in (44).

6.2. SE Performance

The communication channel's capacity in terms of system bandwidth characterizes the SE. The SE of the V2V connection is stated as:

$$\mathrm{SE} = \int_0^\infty \int_0^\infty \ln(1 + \Pr\{\mathrm{SIR}_t^r\}) f_{z_{t2r}}(z_{t2r}) dt dz_{t2r}. \tag{45}$$

The SE of a typical VN in a V2V link with jamming is expressed as:

$$\begin{aligned}\mathrm{SE}_{V2V} &= \mathbf{A}_V \int_0^\infty \int_0^\infty \Pr\{\mathrm{SIR}_V^V > e^t - 1\} f_{z_{V2V}}(z_{V2V}) dt dz_{V2V} \\ &\overset{a}{=} \mathbf{A}_V \int_0^\infty \int_0^\infty L_{I_V}(\bar{s} \setminus z_{V2V}) L_{I_{V_o}}(\bar{s} \setminus z_{V2V}) L_{I_J}(\bar{s} \setminus z_{V2V}) f_{z_{V2V}}(z_{V2V}) dt dz_{V2V}, \end{aligned} \tag{46}$$

where (a) follows by assuming $\bar{s} = P_V^{-1}(e^t - 1) z_V^{-\alpha_V}$ [44]. V2V's SE with uniformly distributed jammers is given by plugging (23), (24), (6), and (27) in (46) and assuming $z_{V2V} = z_V$ and $\bar{s} = P_V^{-1}(e^t - 1) z_V^{-\alpha_V}$. Similarly, V2V's SE with MCP-distributed jammers is given by plugging (23), (24), (6), and (28) in (46) and assuming $z_{V2V} = z_V$ and $\bar{s} = P_V^{-1}(e^t - 1) z_V^{-\alpha_V}$. In a similar fashion, V2U's SE (i.e., SE_{V2U}) is computed. The U-V2X's SE is obtained as $\mathrm{SE} = \mathrm{SE}_{V2V} + \mathrm{SE}_{V2U2V}$, where $\mathrm{SE}_{V2U2V} = \mathbf{A}_U \mathrm{SE}_{V2U} \mathrm{SE}_{U2V}$. Additionally, the SE of a UAV to VN connection can be expressed by SE_{U2V}. It should be noted that SE_{V2U} indicates the reference curve (i.e., the graph of the SE of a LB V2U2V connection), which indicates a 100% affiliation of the VNs with the UAVs (i.e., the pink color line). In a similar way, by eliminating the AP of VNs in (46), a reference curve (i.e., SE of LB V2V connection) is generated, where the VNs have a 100% relationship with the neighboring VNs (i.e., black color line).

7. Results and Discussion

To make a fair comparison with the relevant research papers, the authors considered the network parameters defined in [9], which reflect a realistic real-world environment. Unless otherwise specified, the network settings used to generate the findings are shown in Table 1. V2V, UAV, U-V2X, LB V2U2V, and LB V2V are represented by the red, blue, green, pink, and black color lines. The dashed-dotted line indicates the link with clustered jamming. The dashed line with marker '□', 'o', and 'v' represents the non-clustered jamming with standard deviation of 0°, 2°, and 4°, respectively. Moreover, the solid line with Marker '◇' represents the case with zero jammers and standard deviation of UAV set to 0°.

Note that the results are generated by randomly generating data according to PPP, PLP, and MCP in MATLAB. However, the data can be generated in a similar manner in other software, such as Mathematica. To verify our analysis, we performed simulations by considering realistic network parameters as defined in Table 1.

Table 1. Network parameters and numerical values.

Network Parameter	Numerical Value	Network Parameter	Numerical Value
λ_L	30 km/km^2	$\mathcal{B}$	0.01
μ_V	5/km^2	α_V	3
μ_U	10/km	α_U	3
h_U	80 m	N_U	20
τ	-5 dB	N_V	20
h_b	30 m	f_c	95 GHz
P_V	23 dBm	**B**	3 GHz
P_U	23 dBm	λ_c	2/km^2
P_J	23 dBm	J	2
r_J	100 m	$\sigma, \sigma_x, \sigma_y$	0°
α_J	3	λ_J	4

The simulation outcomes are generated after performing 50,000 successive Monte Carlo runs to back up the findings of the research. In this work, for the first Monte Carlo run, our framework considered that the VN computes its performance in terms of outage and SE in UL and is placed at an origin that receives data from another VN or UAV that is placed randomly in the geographical space. Then, the whole networks' performance is investigated in a similar way by placing VNs and UAVs randomly in the geographical region for up to 50,000 Monte Carlo runs and the results are averaged over the total number of runs (i.e., 50,000). Specifically, our framework in its first Monte Carlo run assumes that the center of the coordinate system has been transformed to the recipient VN's position for each independent trial. Then, the transmitting VN that is closest to a neighboring recipient VN is computed utilizing the distance defined by Euclidean geometry. The maximum average strength of the signal acquired from the transmitting VN at the receiving VN is then calculated. Furthermore, the greatest average strength of the signal acquired from the sender VN at the closest UAV is determined. If the acquired signal from the transmitting VN at the desired VN is greater than the acquired signal strength at the nearby UAV, the sending VN immediately connects with the recipient VN without setting up a connection with the nearest UAV. On the other hand, the sending VN communicates with the UAV for the vice versa case.

Then, assuming that no additional sending VNs (other than the one nearest to the transmitting VN)z are present within the spherical shape of the radius, z_V, we compute the following interfering signals: (i) interference from the VNs at the UAV, (ii) interference from the VNs at the center of the coordinate system, and (iii) interference of the UAVs at the center of the coordinate system. It should be noted that the VN's interference can be broadly classified into two distinct groups: (i) the ones on the same roadway as the recipient destination VN but outside the spherical shape of the radius, z_V; and (ii) those that are on all other roadways (other than the one traversed by the center of the coordinate system) but are located on the exterior of the spherical shape of the radius, z_V. Furthermore, the jamming devices, J, are distributed in a circular disc of a certain radius, r_J, through an MCP, such that the interruption from the jammers located in clusters can be included at the typical node using a distance-dependent PL model with PL exponent given as α_J and transmitting power of the jamming devices given as P_J.

After calculating the received instantaneous SIR while taking into account both direct connection via V2V and propagation via the closest UAV link, the destination VN's OP and SE are evaluated. It should be noted that when the disruptions (i.e., interfering signals) from sites within the spherical shape of the radius, z_V, are not eliminated, the outcomes of the results could be impacted significantly.

Figure 3 shows the OP of a typical VN with τ. It is observed that the probability that a typical VN is in an outage for the U-V2X connection (green color curve), V2U2V connection (blue color curve), and V2V connection (red color curve) increases by increasing the pre-defined SIR threshold value because the obtained SIR is less than the pre-defined τ. The OP

(or conversely, the success probability of a typical node to be in coverage as a function of the SIR threshold, as shown in [9]) for the U-V2X connection is better than the V2V connection or V2U2V connection because the U-V2X connection is in outage when either V2V or V2U2V, or both, are in outage, and is obtained by $\mathcal{O}_{U-V2X} = 1 - (1 - \mathcal{O}_{V2V})(1 - \mathcal{O}_{V2U2V})$. For a fair comparison with the success probability (or conversely, the OP) results in [9], it is observed that the OP of the typical node for the U-V2X, V2V, and V2U2V connection with clustered and non-clustered jammers is at a higher outage value than the OP of the typical node for the U-V2X, V2V, and V2U2V connection without jammers, respectively. Moreover, the OP of the V2U2V connection is lower than the V2V because a lower path loss is obtained for the V2U2V connection (a similar trend and justification exist for the V2U2V and V2V connection curves in the remaining figures). It is also observed that a typical node in CJ U-V2X (green dashed line with square marker) is at a lower outage under clustered jammers in comparison to NCJ U-V2X (green dotted dashed line with square marker) in the presence of uniformly distributed jammers in the given region, because there is a higher probability that clustered jammers restricted to a particular region will reside at a larger distance-dependent path loss from the typical node as compared to non-clustered jammers. Thus, it is important to give higher preference to the jamming attacks of uniformly distributed jammers in comparison to the clustered jammers, as they will severely degrade the network's performance. Moreover, the assumption that clustered jammers generally have a more significant negative impact on network performance compared to non-clustered jammers is not valid. Therefore, serious countermeasures and anti-jamming scenarios must be designed for jamming attacks, especially for non-clustered jamming.

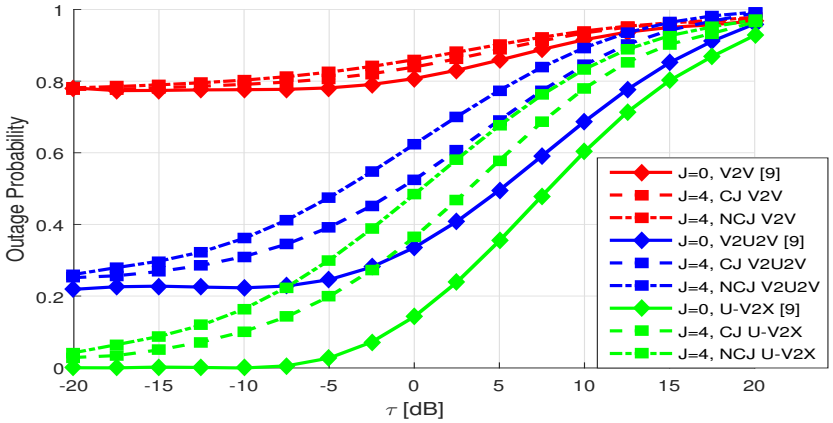

Figure 3. Outage probability of a typical VN as a function of τ with clustered and non-clustered jammers, and without jammers.

Figure 4 shows the OP of a typical VN concerning P_J. It is observed that the probability that a typical VN is in an outage for U-V2X connection, V2U2V connection, and V2V connection increases by increasing P_J because when the jammer's transmission power increases, it increases the jamming interference, which decreases the obtained SIR and results in increasing the OP. The U-V2X connection has a better OP compared to V2V and V2U2V connections, as it considers both the connections (i.e., V2V and V2U connection) to be in an outage. The clustered jammers can result in a lower outage for the CJ U-V2X curve compared to the NCJ U-V2X curve, due to larger path loss from the typical node. Thus, it is critical to prioritize countermeasures against uniformly distributed jammers, as they severely degrade network performance. The conventional assumption that the clustered jammers have a greater impact is inappropriate, requiring efficient anti-jamming scenarios for non-clustered jammers. Additionally, the LB on OP of V2U2V connection (pink color solid line) can be obtained by assuming that all the VNs transmit to the adjacent VNs using UAV connections. In addition to this, the LB on the OP of the V2V connection (black color solid line) can be obtained by assuming none of the VNs transmit to the adjacent VNs using a UAV connection.

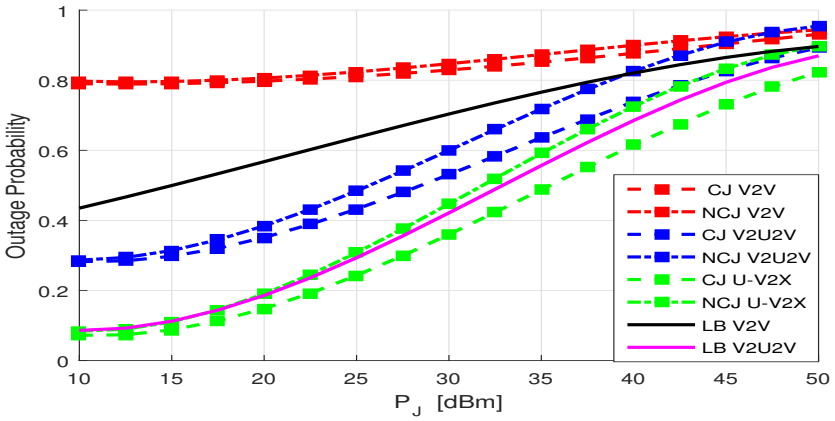

Figure 4. Outage probability of a typical VN as a function of P_J with clustered and non-clustered jammers.

Figure 5 shows the OP of a typical VN concerning the uniformly distributed jammers, J. It is observed that the probability that a typical VN is in an outage for U-V2X connection, V2U2V connection, and V2V connection increases by increasing the number of jammers (i.e., J), because when jammers' values increase, it increases the jammers' transmit power, which decreases the obtained SIR that results in increasing the OP. However, the OP of the U-V2X is lower than the V2V connection or V2U2V connection because the probability of a U-V2X connection is obtained when both the connections, i.e., V2V connection and V2U2V connection, are in an outage. Moreover, the lower bounds on the outage of V2U2V and V2V connections also increase with the increasing number of jammers because LB of V2U2V and LB of V2V are the functions of jammers. It is also noticed that by raising the antenna's variation, U-V2X connection's OP enhances because when antenna's beam-width deviation increases, which decreases an antenna's receiving gain, resulting in decreasing the signal strength and SIR of the signal. Consequently, when the signal strength decreases, the OP of the system increases.

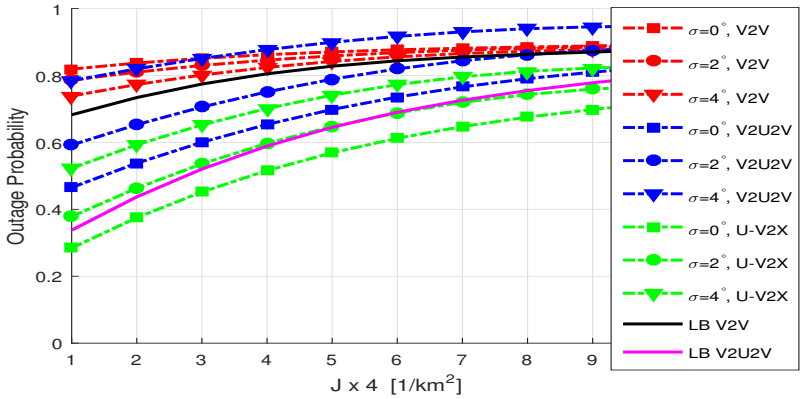

Figure 5. Outage probability of a typical VN as a function of non-clustered jammers with a fluctuating 3D beam width of the antenna.

Figure 6 shows the probability of the VN associating with neighboring VNs and UAVs in V2V and V2U connections, respectively, as a function of UAVs. It can be observed that whenever average UAVs in the network increase, the V2U connection's AP increases because of the decrease in the path loss as compared with the AP of the V2V connection. Moreover, it is also observed that VN's performance in V2U link degrades whenever fluctuations of the antenna increase in comparison with the V2V connection. This is due to the fact that whenever UAV fluctuations increase, it will decrease the antenna's gain as well as the received signal strength.

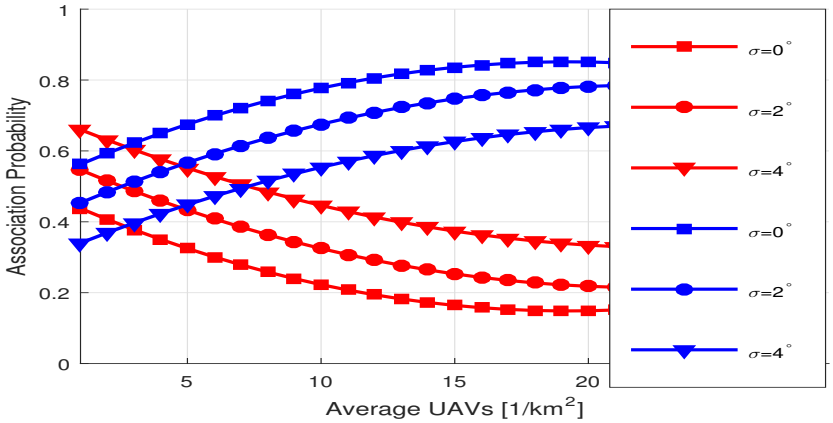

Figure 6. AP of a typical VN exploiting the UAV and the nearest VN against the number of UAVs, for a different number of UAV fluctuations.

Figure 7 shows the OP of the serving node by considering uniformly distributed jammers as a function of UAVs and fluctuating UAV antenna beam width. The probability that a typical VN in V2U2V connection is in outage improves whenever average UAVs increase in the considered space because the path loss between the VN and the UAV connection decreases, resulting in increasing the signal strength obtained as compared with the V2V connection. Furthermore, it is observed that at places with lesser vehicles, roads, and people, UAVs have a greater level of credibility in comparison with the VNs when it comes to setting up communication in intense jamming. It is also observed that the OP of the VN degrades for the U-V2X connection whenever UAV's fluctuations increase in the given system. This is due to the fact that whenever variations in UAV increase, it reduces the gain, received power, and the received SIR (a similar argument may be made for the remaining curves of standard deviation). Moreover, the LB on the OP of the V2V connection remains constant while the LB on the OP of the V2U2V connection degrades whenever average UAVs increase in the system. This is because LB for V2V connection is not the function of UAVs, while the LB for V2U2V connection is the function of UAVs.

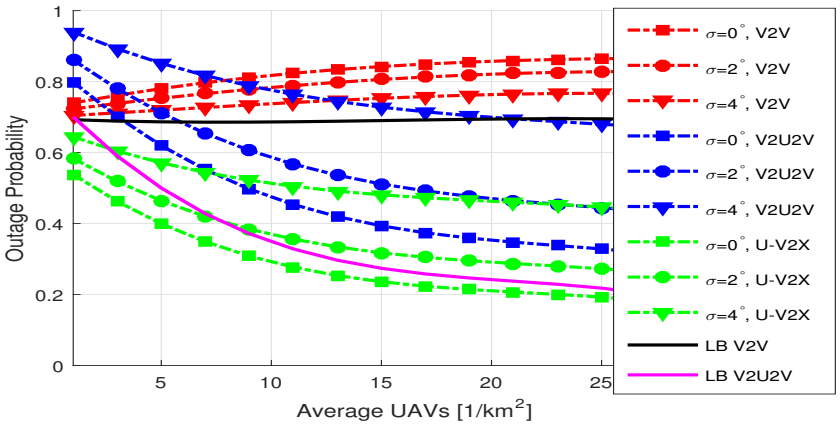

Figure 7. Outage probability of the typical VN considering uniformly distributed jammers as a function of UAVs and fluctuating 3D beam width of the antenna.

Figure 8 shows the OP of the typical VN with clustered and non-clustered jammers and without jammers as a function of VNs. It has been seen that raising the average VNs in the geographical region reduces the V2U2V connection's OP because the path loss between the VN and the UAV connection degrades when compared to the V2V connection resulting in the decrease of the received power and SIR for the V2U2V connection. However, the OP of the U-V2X connection improves with increasing average VNs because the ratio of V2V and V2U2V connection to be in outage improves. Considering a balanced comparison

with the success probability (or inversely, the OP as a function of VNs) outcomes in [9], it is evident that the OP for the typical node in U-V2X, V2V, and V2U2V connections, both with clustered and non-clustered jammers, surpasses the OP for the same connections without jammers. Moreover, it is also observed that the OP of the NCJ U-V2X connection is larger than the CJ U-V2X connection. This is because there is a higher probability that the non-clustered jammers can be located near the typical VN, thus, degrading the network's OP and performance in comparison with the OP of the CJ U-V2X connection.

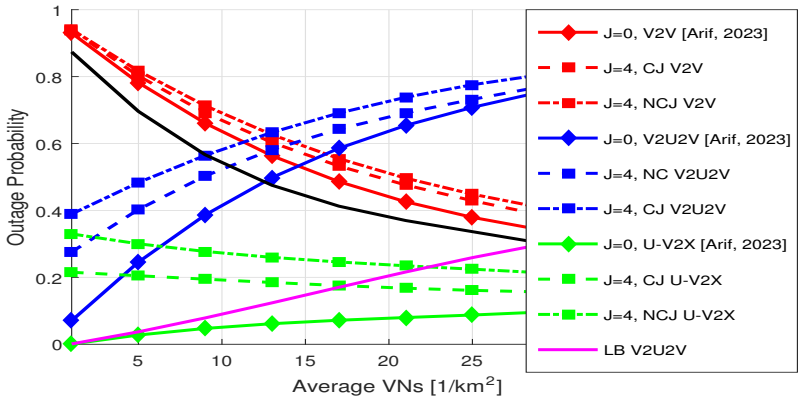

Figure 8. Outage probability of the typical node with clustered and non-clustered jammers and without jammers as a function of VNs.

Figure 9 shows the SE of the VN as a function of P_J by considering clustered and non-clustered jamming interference. It can be observed that the SE of U-V2X, V2U2V, and V2V connection decreases by increasing P_J. This is because when the jammer's transmission power increases, it increases the jamming interference which decreases the obtained SIR, resulting in decreasing the SE of the network. The U-V2X connection has a higher SE when compared with the V2V and V2U2V connections. This is because the U-V2X connection considers that both the connections (i.e., V2V and V2U2V) are in coverage. The SE of the non-clustered jammers is lower in the NCJ U-V2X connection compared with the clustered jammers in the CJ U-V2X connection because there is a larger probability that the uniformly distributed jammers are positioned in the vicinity of the typical VN disrupting the VN's performance. Thus, prioritizing countermeasures against uniformly distributed jammers is very important, as they can degrade the network's performance severely in comparison with the CJ U-V2X connection. Furthermore, the LB on SE of the V2U2V connection (pink color solid line) can be obtained by assuming that all the VNs transmit to the adjacent VNs using a UAV connection and are not in outage. Moreover, the LB for the SE of the V2V connection (black color solid line) can be obtained by assuming none of the VNs transmit to the adjacent VNs using a UAV connection and are not in outage.

Figure 10 shows the SE of a typical VN for the uniformly distributed jammers, J. It can be observed that the SE of the U-V2X, V2U2V, and V2V connection decreases by increasing the number of jammers (i.e., J), because when average jammers in the network increase, it increases the jamming signals that will decrease the obtained SIR that results in decreasing the SE. However, the SE of the U-V2X is better in performance than the V2V connection or V2U2V connection because the SE of the U-V2X connection is obtained by considering that both the connections, i.e., V2V and V2U2V, are in coverage. Moreover, the lower bounds on the SE of the V2U2V and V2V connections also decrease with the increasing number of jammers because LB of V2U2V and LB of V2V are the functions of a number of jammers. It is also observed that the SE of the U-V2X connection degrades whenever the UAV variations increase. This is due to the fact that whenever the deviation of the UAV beam width increases, it decreases the gain of the receiving antenna, resulting in decreasing the received power and SIR of the signal. Thus, when the received SIR decreases, it decreases the system's SE.

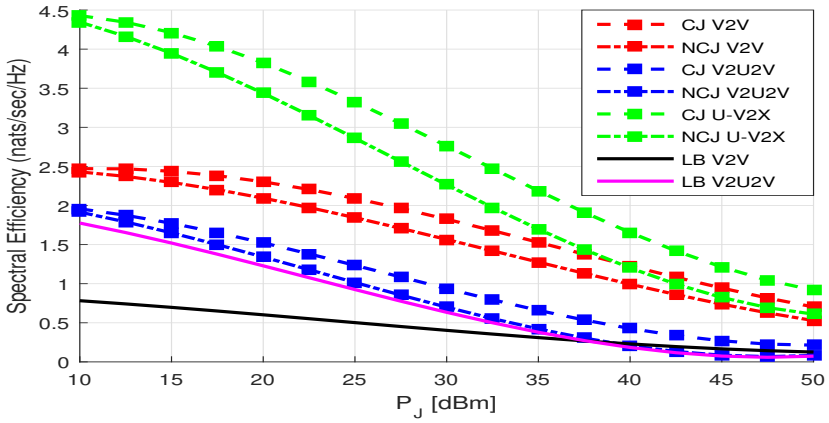

Figure 9. SE of the VN in the presence of clustered and non-clustered jammers as a function of P_J.

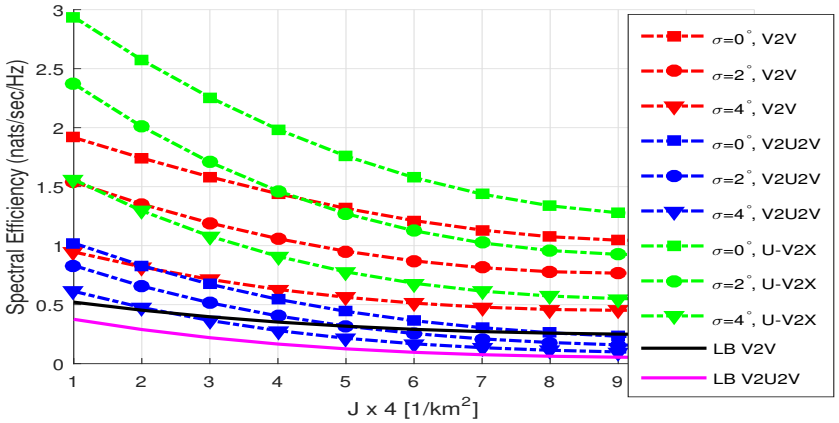

Figure 10. SE of a typical VN as a function of non-clustered jammers with fluctuating 3D beam width of the antenna.

Figure 11 shows the SE of the typical VN by considering uniformly distributed jammers and without jammers as a function of UAVs and fluctuating UAV antenna beam width. The SE of a typical VN in a V2U2V connection improves whenever average UAVs in the considered system increase because the path loss between the VN and the UAV connection decreases, resulting in increasing the signal strength and SIR as compared with the V2V connection. To ensure a fair comparison with the SE outcomes in [9], it is noted that the SE for typical node in U-V2X, V2V, and V2U2V connection without jammers is noticeably higher than the SE for the same connections with non-clustered jammers. It is also observed that the SE of the VN degrades for the U-V2X, V2U2V, and V2V connection whenever UAV variations in the system increase, because it reduces the receiver antenna gain, received power, and the signal strength, resulting in the decrease in SE of the typical node (a similar argument may be made for the remaining curves of standard deviation for SE). Moreover, the LB on the SE of the V2V connection remains constant while the LB on the SE of the V2U2V connection increases whenever average UAVs in the system increase. This is because LB for V2V connection is not the function of UAVs, while the LB for the V2U2V connection is the function of UAVs.

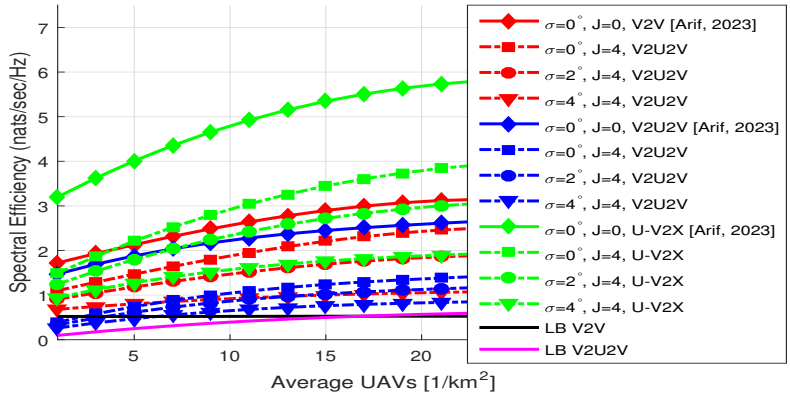

Figure 11. SE of the typical VN in the presence of non-clustered jammers and without jammers as a function of UAVs and fluctuating 3D beam width of the antenna.

Figure 12 shows the SE of the typical VN with and without non-clustered jammers as a function of roads. It has been shown that raising the average roads in the system reduces the SE of the V2U2V connection because the path loss between the VN located around the road and the UAV connection degrades when compared to V2V connection, resulting in the decrease of the received power, SIR, and SE of the V2U2V connection. However, the SE of the NCJ U-V2X connection is higher than the V2U2V and V2V connections. Moreover, it is also observed that the SE of the NCJ U-V2X connection degrades whenever the variations of the UAV increase. This is due to the fact that whenever UAV variations increase in the system, the antenna gain and the SIR decreases. This results in the decrease in the SE of the VN in the network. Considering a fair comparison with the SE of the typical node (with the number of antennas set to 20 and the average roads set to 30 km/km^2) in [9], it is evident that the SE of the typical node in U-V2X connection without jammers surpasses the SE of the same connection with non-clustered jammers.

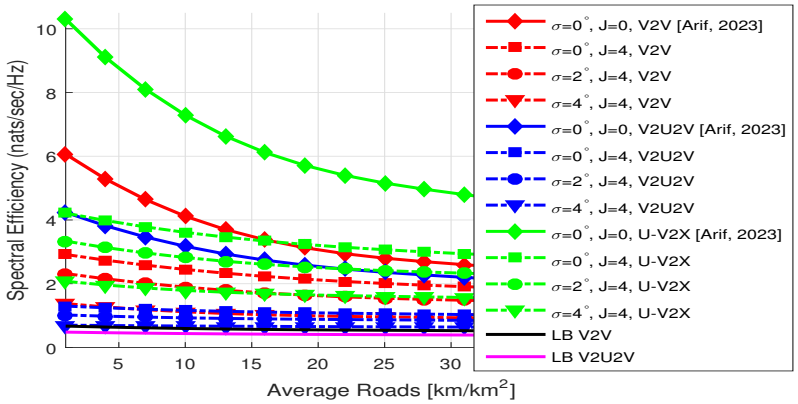

Figure 12. SE of the network with non-clustered jammers and without jammers as a function of roads and fluctuating antenna beam width.

8. Conclusions

In this paper, we modeled non-clustered and clustered jamming in U-V2X communications by considering mm-Waves in the presence of fluctuating 3D antenna beam width. We considered the distribution of roads as PLP, the distribution of VNs as 1D PPP, and the distribution of UAVs as 3D PPP. The fluctuation of 3D antenna beam width is modeled using a normal distribution. The jammers are assumed to follow (i) non-clustered distribution and (ii) clustered distribution. The analytical expressions for the OP of the U-V2X, V2U2V, and V2V connections are analyzed in the presence of jammers and fluctuating antenna beam width. The U-V2X network's performance is quantified in terms of OP and SE for multiple network settings, such as UAVs, VNs, roads, jammers, and jammers' transmission power.

The results revealed that the performance of the U-V2X communications considering mm-Waves is severely degraded in the presence of non-clustered jammers as compared with the clustered jammers. Moreover, the network's performance is further compromised by fluctuations in the 3D beam width of the UAV antenna for the non-clustered jammers. Thus, modeling the fluctuations of 3D beam width of UAV antenna is necessary, especially in the presence of non-clustered jammers. Furthermore, system designers should use additional anti-jamming countermeasures in U-V2X communications that can target non-clustered jammers rather than clustered jammers.

Author Contributions: Conceptualization, M.A.; methodology, M.A.; formal analysis, M.A.; generation of simulation results and comparison, M.A.; validation, M.A. and W.K.; writing—review and editing, M.A. and W.K.; funding acquisition, W.K. All authors have read and agreed to the published version of the manuscript.

Funding: This research was supported by standard development project funded by the Ministry of Science, ICT grant number RS-2023-00228316129820768700001.

Data Availability Statement: No data was used for the research described in the article.

Conflicts of Interest: The authors declare no conflict of interest.

Appendix A. Derivation of (6)

The cumulative distributive function (CDF), $F_{z_V}(z_V)$, of the distance to the VN, could be determined by assuming that the likelihood of the VNs located on roadways in a sphere of radius z_V, (i.e., $\Pr\{\mathbf{N}(\mathbf{S}(o, z_V)) = 0\}$). Similarly, the probability of the VNs on a length of roadways from $-z_{V_o}$ and z_{V_o} crossing the center of the coordinate system is 0 (i.e., $\Pr\{\mathbf{N}_{z_{V_o}}(-z_{V_o}, z_{V_o}) = 0\}$). The CDF is expressed as [15]:

$$F_{z_V}(z_V) = 1 - \Pr\{z_V > x\} = 1 - \underbrace{\Pr\{\mathbf{N}(\mathbf{S}(o, z_V)) = 0\}}_{\Xi_a} \underbrace{\Pr\{\mathbf{N}_{z_{V_o}}(-z_{V_o}, z_{V_o}) = 0\}}_{\Xi_b}, \quad \text{(A1)}$$

where the chance that VNs in a spherical region with the radius z_V is zero is given by Ξ_a, and the chance that the VN on a segment of the highway that spans from $-z_V$ to the coordinate system's center and then from coordinate's center to z_V is zero is given by Ξ_b. Then, we compute the probability of a VN shown to be zero on each m-th highway. ($\Pr\{N_V(\text{Road}_m) = 0\}$). Ξ_a is expressed as:

$$\begin{aligned} \Xi_a =& \sum_{k=0}^{\infty} \Pr\{\mathbf{N}_{\text{Roads}}(\mathbf{S}(o, z_V)) = k\} \times \prod_{m=1}^{k} \Pr\{N_V(\text{Road}_m) = 0\} \\ =& \underbrace{\sum_{k=0}^{\infty} \frac{\exp(-2\pi\lambda_L z_V)(2\pi\lambda_L z_V)^k}{k!}}_{\top_1} \underbrace{\left(\int_{-z_V}^{z_V} \frac{e^{-2\mu_V\sqrt{z_V^2 - y^2}}}{2z_V} dy \right)^k}_{\top_2}, \end{aligned} \quad \text{(A2)}$$

where the probability in $\top_1$ may be determined by considering that k roads that are spread out uniformly employing PPP with the mean nodes given as $2\pi\lambda_L z_V$ and fall inside a spherical shape with radius z_V, and the $\top_2$ probability can be obtained by considering that VNs across each of the m-th highways possess a uniform distribution with the length of $2\mu_V\sqrt{z_V^2 - y^2}$.

$$\Xi_a = \exp(-2\pi\lambda_L z_V) \sum_{k=0}^{\infty} \frac{\left(\pi\lambda_L \int_{-z_V}^{z_V} e^{-2\mu_V\sqrt{z_V^2 - y^2}} dy \right)^k}{k!} \quad \text{(A3)}$$

where (A3) is the result of simple mathematics. After further simplifications, we obtain:

$$\Xi_a = \exp(-2\pi\lambda_L z_V)\exp\left(\pi\lambda_L \int_{-z_V}^{z_V} e^{-2\mu_V\sqrt{z_V^2-y^2}}dy\right) \tag{A4}$$

where (A4) is produced by the assumption $\sum_{k=0}^{\infty}\frac{\mathcal{Y}^k}{k!} = e^{\mathcal{Y}}$. Furthermore, Ξ_a is given as:

$$\Xi_a = \exp\left(-2\pi\lambda_L \int_0^{z_V}\left(1-e^{-2\mu_V\sqrt{z_V^2-y^2}}\right)dy\right) \tag{A5}$$

where (A5) is obtained via the following mathematical techniques. In a similar fashion, the second term in (A1), $\Xi_b = \exp(-2\mu_V z_V)$ is obtained. The final expression is given by plugging Ξ_a and Ξ_b in (A1) and is expressed as:

$$F_{z_V}(z_V) = 1-\exp\left(-2\pi\lambda_L\int_0^{z_V} 1-e^{-2\mu_V\sqrt{z_V^2-y^2}}dy\right)\exp(-2\mu_V z_V). \tag{A6}$$

Appendix B. Derivation of (27)

The interference of the uniformly distributed jammers at the receiving node can be determined by the Laplace transform of interference of the uniformly distributed jammers as [34]:

$$\begin{aligned}
L_{I_J^{NC}}(\tau) &\overset{a}{=} \mathbb{E}_{g,z}\left\{\exp\left(-\frac{\tau\|z_r-z_t\|^{-\alpha_r}}{P_t}\sum_{j\in I_J^{NC}} P_J g_j\|z_r-z_j\|^{-\alpha_r}\right)\right\}\\
&\overset{b}{=} \mathbb{E}_z\left\{\prod_{j\in I_J^{NC}}\mathbb{E}_g\left\{\exp\left(-\frac{\tau\|z_r-z_t\|^{-\alpha_r}}{P_t}P_J g_j\|z_r-z_j\|^{-\alpha_r}\right)\right\}\right\}\\
&\overset{c}{=} \mathbb{E}_z\left\{\prod_{j\in I_J^{NC}}\frac{1}{1+\tau\Delta\left(\frac{D_j}{z}\right)^{-\alpha_r}}\right\}\\
&\overset{d}{=} \exp\left\{-2\pi\lambda_r\int_{z_0}^{z_1}\frac{D_j dD_j}{1+\Delta\left(\frac{D_j}{\tau^{1/\alpha_r}z}\right)^{\alpha_r}}\right\}\\
&\overset{e}{=} \exp\left\{-\pi\lambda_r\tau^{2/\alpha_r}\Delta z^2\int_{\left(\frac{z_0}{\tau^{1/\alpha_r}z}\right)^2}^{\left(\frac{z_1}{\tau^{1/\alpha_r}z}\right)^2}\frac{dw}{1+w^{\alpha_r/2}}\right\},
\end{aligned} \tag{A7}$$

where (a) follows by plugging $s = \frac{\|z_r-z_j\|^{\alpha_r}}{P_t}$ in (16), (b) follows by the independent point-process assumption, (c) follows by exponentially distributed Rayleigh fading gains and considering $D_j = \|z_r-z_j\|$, $z = \|z_r-z_t\|$, and $\Delta = \frac{P_J}{P_t}$, (d) follows by applying probability generating function (PGF) property to polar coordinates, i.e., z_0 and z_1 indicate the initial and final limits of the integration, respectively, and (e) follows by changing the variables, i.e., $w = \left(\frac{D_i}{\tau^{1/\alpha_r}z}\right)^2$. The final equation in (27) is obtained by applying the limits to A7.

Appendix C. Derivation of (28)

The interference of the clustered jammers with MCP distribution is evaluated by following [11,45] and is derived as:

$$L_{I_j^C} = \varkappa_a \times \varkappa_b \tag{A8}$$
$$= \overbrace{\exp\{-\lambda_c \int_0^z (1-\exp\{-J\mathrm{Y}(t,y)\})dy\}}^{\varkappa_a} \times \overbrace{\int_0^z \exp\{-J\mathrm{Y}(t,y)\}f(y)dy}^{\varkappa_b},$$

where $\mathrm{Y}(t,y) = \int_0^z \frac{g(x-y-t)}{g(x-y-t)+g(t)/\tau} f(x)dx$ and $\varkappa_a$ is the PGF of MCP-distributed jammers. The PGF is simplified as:

$$\begin{aligned}
\varkappa_a &= \exp\left\{-\lambda_c \int_0^z \left(1-\exp\left\{-\lambda_c \int_0^z \frac{g(x-y-t)}{g(x-y-t)+g(t)/\tau} f(x)dx\right\}\right)dy\right\} \\
&\overset{a}{=} \exp\left\{-\lambda_c \int_0^z \left(1-\exp\left\{\int_0^z -\frac{Jg(y)f(x)dx}{g(y)+g(t)/\tau}\right\}\right)dy\right\} \\
&\overset{b}{=} \exp\left\{-2\pi\lambda_c \int_0^z \left(1-\exp\left\{\frac{-Jy^{-\alpha_r}}{y^{-\alpha_r}+t^{-\alpha_r}/\tau}\right\}\right)ydy\right\} \\
&\overset{c}{=} \exp\left\{-\lambda_c \pi \tau^{2/\alpha_r} z^2 \int_0^z \left(1-\exp\left\{\frac{-J}{1+\omega^{\alpha_r/2}}\right\}\right)d\omega\right\},
\end{aligned}$$

where (a) is obtained via changing the variables in the system, $(b)$is obtained by simple mathematics, and (c) is obtained by assuming $\omega = \tau^{-2/\alpha_r} t^{-2} y^2$. In addition to this, $\varkappa_b$ follows by simple mathematics [45] as $\varkappa_b = \int_0^z \exp\{-\mathbf{J}\mathrm{Y}(t,y)\}f(y)dy = \exp\{-\mathbf{J}z^2\tau^{2/\alpha_r}\frac{2\pi^2}{\alpha_r}$ $\csc(2\pi/\alpha_r)\}$, where $\mathbf{J} = \lambda_c J(\pi r_J^2)^{-1}$. Plug $\varkappa_a$ and $\varkappa_b$ in $L_{I_j^C}$ to obtain the final expression of MCP-distributed jammers.

References

1. Traspadini, A.; Giordani, M.; Zorzi, M. UAV/HAP-assisted vehicular edge computing in 6G: Where and what to offload? In Proceedings of the 2022 Joint European Conference on Networks and Communications & 6G Summit (EuCNC/6G Summit), Grenoble, France, 7–10 June 2022; IEEE: Piscataway, NJ, USA, 2022; pp. 178–183. [CrossRef]
2. Mitsuhashi, T.; Kawamoto, Y.; Kato, N. Controlling UAV for maximizing the number of receiver vehicles in intelligent transportation systems. In Proceedings of the 2019 IEEE Global Communications Conference (GLOBECOM), Waikoloa, HI, USA, 9–13 December 2019; IEEE: Piscataway, NJ, USA, 2019; pp. 1–6. [CrossRef]
3. 3GPP TR36.885. Study on LTE-Based V2X Services (Release 14). In *Technical Specification Group Services System*; ETSI: Sophia Antipolis, France, 2016.
4. Cao, Y.; Xu, S.; Liu, J.; Kato, N. Toward smart and secure V2X communication in 5G and beyond: A UAV-enabled aerial intelligent reflecting surface solution. *IEEE Veh. Technol. Mag.* **2022**, *17*, 66–73. [CrossRef]
5. Dhawankar, P.; Agrawal, P.; Abderezzak, B.; Kaiwartya, O.; Busawon, K.; Raboacă, M.S. Design and numerical implementation of V2X control architecture for autonomous driving vehicles. *Mathematics* **2021**, *9*, 1696. [CrossRef]
6. Ding, Y.; Huang, Y.; Tang, L.; Qin, X.; Jia, Z. Resource allocation in V2X communications based on multi-agent reinforcement learning with attention mechanism. *Mathematics* **2022**, *10*, 3415. [CrossRef]
7. Lansky, J.; Rahmani, A.M.; Hosseinzadeh, M. Reinforcement Learning-Based Routing Protocols in Vehicular Ad Hoc Networks for Intelligent Transport System (ITS): A Survey. *Mathematics* **2022**, *10*, 4673. [CrossRef]
8. Ma, R.; Yang, W.; Zhang, Y.; Liu, J.; Shi, H. Secure mmWave communication using UAV-enabled relay and cooperative jammer. *IEEE Access* **2019**, *7*, 119729–119741. [CrossRef]
9. Arif, M.; Hasna, M.O. Analysis of fluctuations of antenna pattern in U-V2X communications. *Phys. Commun.* **2023**, *58*, 102066. [CrossRef]
10. Afshang, M.; Dhillon, H.S. Poisson cluster process based analysis of HetNets with correlated user and base station locations. *IEEE Trans. Wirel. Commun.* **2018**, *17*, 2417–2431. [CrossRef]
11. Ganti, R.K.; Haenggi, M. Interference and outage in clustered wireless Ad Hoc networks. *IEEE Trans. Inf. Theory* **2009**, *55*, 4067–4086. [CrossRef]
12. Chun, Y.J.; Hasna, M.O.; Ghrayeb, A. Modeling heterogeneous cellular networks interference using poisson cluster processes. *IEEE J. Sel. Areas Commun.* **2015**, *33*, 2182–2195. [CrossRef]

13. Chun, Y.J.; Hasna, M.O. Analysis of heterogeneous cellular networks interference with biased cell association using Poisson cluster processes. In Proceedings of the 2014 International Conference on Information and Communication Technology Convergence (ICTC), Busan, Republic of Korea, 22–24 October 2014; IEEE: Piscataway, NJ, USA, 2014; pp. 319–324. [CrossRef]
14. Arif, M.; Kim, W.; Qureshi, S. Interference Characterization in Cellular-Assisted Vehicular Communications With Jamming. *IEEE Access* **2022**, *10*, 42469–42480. [CrossRef]
15. Sial, M.N.; Deng, Y.; Ahmed, J.; Nallanathan, A.; Dohler, M. Stochastic geometry modeling of cellular V2X communication over shared channels. *IEEE Trans. Veh. Technol.* **2019**, *68*, 11873–11887. [CrossRef]
16. Dhillon, H.S.; Chetlur, V.V. Poisson Line Cox Process: Foundations and Applications to Vehicular Networks. *Synth. Lect. Learn. Netw. Algorithms* **2020**, *1*, 1–149. [CrossRef]
17. Chetlur, V.V.; Dhillon, H.S. On the load distribution of vehicular users modeled by a Poisson line Cox process. *IEEE Wirel. Commun. Lett.* **2020**, *9*, 2121–2125. [CrossRef]
18. Andrews, J.G.; Ganti, R.K.; Haenggi, M.; Jindal, N.; Weber, S. A primer on spatial modeling and analysis in wireless networks. *IEEE Commun. Mag.* **2010**, *48*, 156–163. [CrossRef]
19. Andrews, J.G.; Gupta, A.K.; Dhillon, H.S. A primer on cellular network analysis using stochastic geometry. *arXiv* **2016**, arXiv:1604.03183. https://doi.org/10.48550/arXiv.1604.03183.
20. Osanaiye, O.; Alfa, A.S.; Hancke, G.P. A statistical approach to detect jamming attacks in wireless sensor networks. *Sensors* **2018**, *18*, 1691. [CrossRef] [PubMed]
21. Del-Valle-Soto, C.; Mex-Perera, C.; Nolazco-Flores, J.A.; Rodríguez, A.; Rosas-Caro, J.C.; Martínez-Herrera, A.F. A low-cost jamming detection approach using performance metrics in cluster-based wireless sensor networks. *Sensors* **2021**, *21*, 1179. .: 10.3390/s21041179. [CrossRef]
22. Savva, M.; Ioannou, I.; Vassiliou, V. Fuzzy-logic based IDS for detecting jamming attacks in wireless mesh IoT networks. In Proceedings of the 2022 20th Mediterranean Communication and Computer Networking Conference (MedComNet), Pafos, Cyprus, 1–3 June 2022; IEEE: Piscataway, NJ, USA, 2022; pp. 54–63. [CrossRef]
23. Zhang, K.; Zhang, G.; Yu, X.; Hu, S.; Li, M. Clustering the sensor networks based on energy-aware affinity propagation. *Comput. Netw.* **2022**, *207*, 108853. [CrossRef]
24. Zhou, Z.; Wei, Y. The Influence of Automatic Gain Control on Narrowband Frequency Domain GPS Anti-Jamming Receiver. In Proceedings of the 2021 IEEE 21st International Conference on Communication Technology (ICCT), Tianjin, China, 6–10 December 2021; IEEE: Piscataway, NJ, USA, 2021; pp. 497–501. [CrossRef]
25. Moussa, M.; Osman, A.; Tamazin, M.; Korenberg, M.J.; Noureldin, A. Direction of arrival estimation of GPS narrowband jammers using high-resolution techniques. *Sensors* **2019**, *19*, 5532. [CrossRef]
26. Li, X.; Zhou, W.; Peng, J.; Shan, H. Joint beamwidth and resource optimization in ultra-dense MmWave D2D communications. *Wirel. Netw.* **2023**, *29*, 2093–2104. [CrossRef]
27. Khan, M.Q.; Gaber, A.; Schulz, P.; Fettweis, G. Machine Learning for Millimeter Wave and Terahertz Beam Management: A Survey and Open Challenges. *IEEE Access* **2023**, *11*, 11880–11902. [CrossRef]
28. Dong, Y.; He, C.; Wang, Z.; Zhang, L. Radio map assisted path planning for UAV anti-jamming communications. *IEEE Signal Process. Lett.* **2022**, *29*, 607–611. [CrossRef]
29. Ma, N.; Xu, K.; Xia, X.; Wei, C.; Su, Q.; Shen, M.; Xie, W. Reinforcement learning-based dynamic anti-jamming power control in UAV networks: An effective jamming signal strength based approach. *IEEE Commun. Lett.* **2022**, *26*, 2355–2359. [CrossRef]
30. Yu, J.; Gong, Y.; Fang, J.; Zhang, R.; An, J. Let Us Work Together: Cooperative Beamforming for UAV Anti-Jamming in Space-Air-Ground Networks. *IEEE Internet Things J.* **2022**, *9*, 15607–15617. [CrossRef]
31. Wang, H.; Ding, G.; Chen, J.; Zou, Y.; Gao, F. UAV Anti-Jamming Communications with Power and Mobility Control. *IEEE Trans. Wirel. Commun.* **2022**, *22*, 4729–4744. [CrossRef]
32. Rahmati, A.; Hosseinalipour, S.; Yapıcı, Y.; He, X.; Güvenç, I.; Dai, H.; Bhuyan, A. Dynamic interference management for UAV-assisted wireless networks. *IEEE Trans. Wirel. Commun.* **2021**, *21*, 2637–2653. [CrossRef]
33. Amuru, S.; Dhillon, H.S.; Buehrer, R.M. An error probability analysis of jamming against wireless networks. In Proceedings of the 2016 IEEE International Conference on Communications (ICC), Kuala Lumpur, Malaysia, 23–27 May 2016; IEEE: Piscataway, NJ, USA, 2016; pp. 1–6. [CrossRef]
34. Haroon, M.S.; Chae, S.H.; Jeon, S.W. Outage analysis for multi-radio heterogeneous networks in the presence of aerial jammers. *ICT Express* **2023**, *in press*. [CrossRef]
35. Dabiri, M.T.; Hasna, M. Pointing Error Modeling of mmWave to THz High-Directional Antenna Arrays. *IEEE Wirel. Commun. Lett.* **2022**, *11*, 2435–2439. [CrossRef]
36. Dabiri, M.T.; Hasna, M. 3D Uplink Channel Modeling of UAV-based mmWave Fronthaul Links for Future Small Cell Networks. *IEEE Trans. Veh. Technol.* **2022**, *72*, 1400–1413. [CrossRef]
37. Dabiri, M.T.; Safi, H.; Parsaeefard, S.; Saad, W. Analytical channel models for millimeter wave UAV networks under hovering fluctuations. *IEEE Trans. Wirel. Commun.* **2020**, *19*, 2868–2883. [CrossRef]
38. 3GPP TR 38.901 V14.1.1. Study on channel model for frequencies from 0.5 to 100 GHz (Release 17). In *Technical Specification Group Services System*; ETSI: Sophia Antipolis, France, 2017.
39. Balanis, C.A. *Antenna Theory: Analysis and Design*; John Wiley & Sons: Hoboken, NJ, USA, 2015.

40. Dabiri, M.T.; Rezaee, M.; Yazdanian, V.; Maham, B.; Saad, W.; Hong, C.S. 3D channel characterization and performance analysis of UAV-assisted millimeter wave links. *IEEE Trans. Wirel. Commun.* **2020**, *20*, 110–125. [CrossRef]
41. Chiu, S.N.; Stoyan, D.; Kendall, W.S.; Mecke, J. *Stochastic Geometry and Its Applications*; John Wiley & Sons: Hoboken, NJ, USA, 2013. [CrossRef]
42. Novlan, T.D.; Dhillon, H.S.; Andrews, J.G. Analytical modeling of uplink cellular networks. *IEEE Trans. Wirel. Commun.* **2013**, *12*, 2669–2679. [CrossRef]
43. Olver, F.W.; Lozier, D.W.; Boisvert, R.F.; Clark, C.W. *NIST Handbook of Mathematical Functions Hardback and CD-ROM*; Cambridge University Press: Cambridge, UK, 2010.
44. Andrews, J.G.; Baccelli, F.; Ganti, R.K. A tractable approach to coverage and rate in cellular networks. *IEEE Trans. Commun.* **2011**, *59*, 3122–3134. [CrossRef]
45. Wang, Y.; Zhu, Q. Modeling and analysis of small cells based on clustered stochastic geometry. *IEEE Commun. Lett.* **2017**, *21*, 576–579. [CrossRef]